Authors Response

We thank Amanda Maycock and the two anonymous referees for the interest in our study and the careful reading which helped to improve the paper. We hope that our replies to the comments from the referees answer the issues in a satisfying way, and that the changes in the manuscript motivated by the comments improved the paper. This document is structured as follows: First our point-by-point response to the first review, followed by the response to the second review (beginning at page 8), each in the following order: 1.) comment from the reviewer, 2.) our response and 3.) the changes in the manuscript. Changes marked in blue refer to the first review, cyan coloured text refers to the second review. A marked up manuscript version is attached below the responses.

Point-by-point response to the first review

Comment 1: Cyclone tracking: P5, lines 6 to 11. I appreciated the detailed description of the cyclone tracking algorithm but I am concerned about the effect of the projection and interpolation. The final composited feature in static stability looks like a North-South dipole. I am wondering what the effect of the original grid and interpolation does to this feature. E.g., does it enhance the dipole?

Reply to comment 1: The Lambert projection is solely part of the tracking algorithm. Once the tracks are defined, all data like e.g. the quasi-horizontal fields of the maximum in static stability N^2 above the thermal tropopause are extracted from the original ECMWF latitude-longitude-grid. Therefore the Lambert projection has no effect on the analysis of the North-South dipole feature of the static stability.

The interpolation onto an area-preserving Lambert projection is done based on the work of Hanley and Caballero (2012) who chose this specific projection to counteract the bias in effective zonal resolution when searching for local minima in the mean sea level pressure field (or any field for that reason). The higher zonal resolution at higher latitudes (with reference to the geometric distance between grid points) could be regarded as an advantage, representing denser information, but at the same time it represents an inconsistency between high and low latitudes. The interpolation on to the area preserving Lambert projection with uniform geometric grid (with 28 km grid spacing, representing a form of lowpass-filter for the higher latitudes) counteracts that fact, achieving a more consistent cyclone track density over the whole area.

Comment 2: Composites of cyclones: P6, line 11. Do you mean cylindrical rather than spheric? The data you have is on an equidistant grid (Is this gridding only done for the cyclone tracking or is this gridded data used for the subsequent composites). I am confused about which data is being interpolated to the red pillar since the underlying grey grid in figure 2 is not equidistant.

Reply to comment 2: The basis for the interpolation is defined by the rotation of a spherical polar coordinate surface onto the centre of a tracked cyclone. The pillar of gridded data interpolated on the new rotated grid with the height coordinate dz relative to the tropopause could indeed be described as a cylindrical polar coordinate system. The underlaying grey grid in Figure 2 represents the original latitude-longitude grid as provided by the ECMWF with equidistant latitude and longitude grid spacing, but the geometric distance depends on the latitude (the aforementioned bias in zonal resolution). These original fields are interpolated onto the rotated new spherical coordinates with spherical cap of 15° (red area). This achieves comparable areas independent of where each cyclone centre is located. We reworded the specific paragraph describing the interpolation method as follows:

Changes in the manuscript:

Page 7 Line 4: We select a subset of the gridded data as provided by the ECMWF for each cyclone by rotating the pole of a spheric polar coordinate system $(\Theta,\ \phi)$ onto the centre of the cyclone and interpolated the original data onto that new grid. The horizontal resolution of the new coordinate system is set to 0.25° and the spherical cap radius to $\Theta_{max} = 15^\circ$ ~~(Fig. 2)~~. The radius is chosen such that all relevant features around the cyclone centre are covered. Figure 2 illustrates the inter-

polation of the data from the original latitude-longitude grid provided by the ECMWF (light grey area for the whole sphere, dark grey for the limited area used in this study) onto an arbitrarily placed new spherical polar coordinate system (orange area).

Comment 3: LC1 and LC2 case studies: Seeing the case studies is helpful in interpreting the composites. Care should be taken in discussing the static stability strength, particularly with the discontinuities that are seen as a result of the analysis in fig 3c and 5c. I would be interested in seeing the average of N^2 (as opposed to N^2_{max}) in the region 3 km above the tropopause. Side note: Add your definition of N^2_{max} to the caption in Fig 3c.

Reply to comment 3: We agree that a detailed discussion of the sub-synoptic-scale or even sub-meso scale features should be treated with caution when using a certain TIL strength definition, due to the discontinuities described. We nevertheless choose the maximum in N^2 above the tropopause as the TIL-strength definition for this study, because we are working with fine grid spacing data, and we want to highlight the variability of the static stability on different scales on one hand and show the difficulties when working with a certain definition of the TIL-strength on the other hand. The average within a certain vertical extent above the tropopause does not only filter a lot of information by default, but in particular for the feature of N^2 above the tropopause, because we know from previous work that larger maxima in N^2 above the tropopause tend to have a smaller vertical extent. Therefore an average over a defined vertical range above the tropopause could have a particular smoothing effect concerning even the large scale variability. We plotted the average of N^2 within 3 km above the tropopause for our case studies for comparison (Figure R1 and R2). Importantly, the analysis using a 3 km-averaged static stability shows very similar locations of the maximum TIL-structures on a synoptic scale, with the largest values in the regions of cyclonic wrap-up around the cyclone centre of air masses originating from lower latitudes. We did not add these plots to the manuscript, but we added the description of an average-based TIL strength definition at the end of section 2.1, to clarify that we deliberately decided to use another definition. We furthermore added the definition of the TIL strength to the caption in Figure 3.

Changes in the manuscript:

Page 4 Line 18: We ~~do this~~ use this specific TIL strength definition, since the high resolution data shows large variability in the UTLS region, with often several maxima evident above the tropopause. Therefore, we find this definition of the TIL strength to be preferable over e.g. the first maximum in static stability above a threshold (4×10^{-4} s^{-2}, e.g., Gettelman and Wang, 2015). Another way to describe the static stability above the tropopause is to calculate the mean value of N^2 over a predefined vertical extent relative to the tropopause (e.g., Kunkel et al., 2014). While such a TIL strength definition achieves very similar results on a synoptic scale to the ones we will describe in Sect. 3, it also filters a lot of small scale variability and therefore partly neutralises the advantage of analysing high resolution data.

Page 9 Fig. 3 caption: Evolution of a baroclinic wave breaking event as seen in ECMWF IFS analysis data. The middle row represents the 14th of October 2014 at 06:00 UTC~~,~~ (the point in time of maximum cyclone intensity), the upper and lower row show the situation 24 hours prior and past the maximum intensity. Column (a) shows the pressure at mean ~~seal~~ sea level ~~(solid lines $p_{msl} < 1013$ hPa, dashed $p_{msl} > 1013$ hPa, dotted $p_{msl} = 1013$ hPa)~~(solid lines $p_{msl} \leq 1013$ hPa, dashed lines $p_{msl} > 1013$ hPa, in steps of 5 hPa), (b) the IPV on 330 K, (c) the maximum of static static stability N^2_{max} within 3 km above the thermal tropopause as indicator for the TIL strength, and (d) the relative vorticity at lapse rate tropopause height. Blue lines in middle row show 40 and 50 m s^{-1} horizontal windspeed isolines at 200 hPa. Dashed black line shows the path of migration of the tracked cyclone, with the position of the cyclone centre at the point in time of the meteorological field displayed marked by the black x. Black circles show the 15° radius used for the composites. Note the deformation of the circles due to the mercator projection.

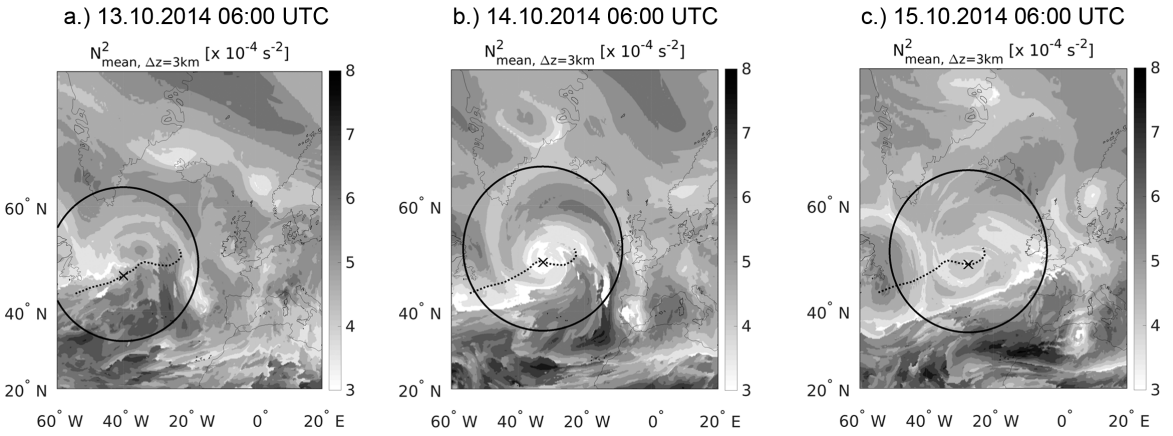

Figure R1. Evolution of the N^2 average based TIL strength for the LC2 resembling baroclinic wave breaking event. The grey contour shows the average of static stability over the vertical extent of 3 km above the thermal tropopause. Figure 1a) shows the TIL strength 24 hours before maximum intensity of the surface cyclone, b) at maximum intensity and c) 24 hours later.

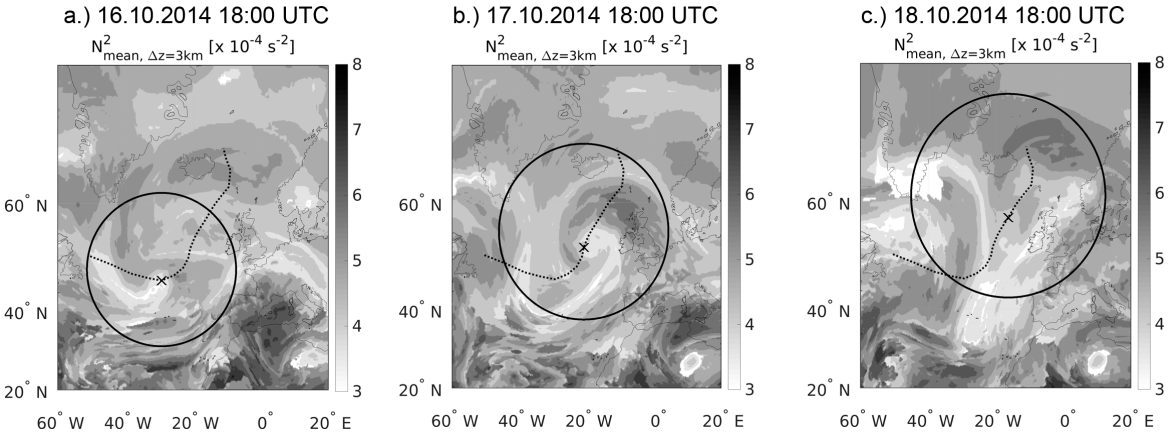

Figure R2. As in Figure R1 but for the LC1 resembling baroclinic wave breaking event.

Comment 4: In figure 4, it may be more helpful to show the cross section at some latitude north of the cyclone centre since this is the region where there is an enhancement in N^2.

Reply to comment 4: We chose this cross-section in particular because it shows the small-scale stratospheric intrusion at around 12° W which is also visible as a discontinuity in the N^2_{max} contour plot in Figure 3 in the middle row. It furthermore covers the tropopause jump between 30° W and 40° W. Both characteristics are the ones described in the paragraph associated with Figure 4. We included an additional cross-section (Figure R3) north of the cyclone centre into the manuscript to furthermore illustrate the variability of N^2 above the tropopause in the region of interest.

Changes in the manuscript:
Page 10 Line 25: The vertical cross-section in Fig. 4b shows the TIL structures at 60° N on the same day and north of the cyclone centre. It illustrates that the regions of enhanced static stability exhibit less variability at this latitude. They are located above the ridge between 40° W and 10° W, with the wave-like horizontal pattern that is also visible in Fig. 3c.

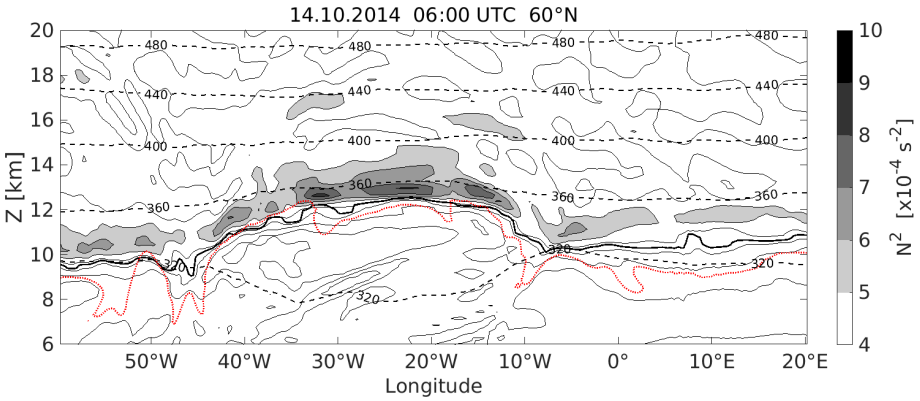

Figure R3. Vertical crosssection over the North Atlantic on 14.10.2014 at 06:00 UTC at 60° N. The filled contour as well as the thin solid black contour lines show static stability N^2 in steps of $1 \times 10^{-4}\mathrm{s}^{-2}$, dashed black lines show isentropes. The bold solid black line indicates the lapse rate tropopause, the dotted red line shows the 2 pvu isoline of potential vorticity.

Comment 5: Composite analysis: I have some concerns about the compositing the values of N^2_{max} and artefacts that might arise as a result of this. Have you looked at a number of cyclones in your composite to make sure that the features in N?2 are indeed present in most of them?

Reply to comment 5: This is a very valid concern which we shared during the data evaluation, especially since we know about the sensitivity of the result on the TIL-strength definition. We did in fact look at a large number of cyclones independently. While there is a large variability in the evolution of the upper tropospheric / lower stratospheric wrap-up around the cyclone centre (caused by the variability of the background flow, the cyclone evolution and the wave activity in the UTLS, as well as the variety of mechanism which influence the static stability at tropopause altitude). Most of the cyclones and especially the strong ones exhibit a comparable evolution of the static stability above the tropopause, with the wrapped-up North-South-dipole as the synoptic to mesoscale shaping. We furthermore estimate the mentioned discontinuities in the TIL-strength due the reasons described in the last paragraph of subsection 3.1 to be small and infrequent enough to be negligible for the large scale composite analysis. We updated Figure 11 and added Fig 12 to the manuscript with a set of vertical tropopause-based

cross-section composites of S^2 and N^2, which further illustrate the issue in a more comprehensive way. The plots complement Figure 9 and Figure 10b for different rotation angles around the cyclone centre, and while all these cross-section composites are solely based on the lapse rate tropopause definition, they do agree very well with the composites derived from the quasi-horizontal fields of the individual cyclones that depend on the definition of the TIL-strength and the strength of the wind shear (maximum of N^2 (Fig. 7b) / S^2 (Fig. 12) within 3 km above the tropopause). We added a description of this comparison to the manuscript.

Changes in the manuscript:

Page 19 Figure 11 caption: ~~Composite of flow features for the 76 strong cyclones with $p_{msl,\,min} \leq 990$ hPa at the point in time of maximum intensity. Left panel: composite of the maximum in vertical wind shear S^2_{max} found within 3 km above the lapse rate tropopause for each cyclone. The black arrow indicates the position of the vertical cross-sections in Fig. 9. Right panel: composite of the absolute height difference between the maximum in static stability N^2_{max} and the maximum in vertical wind shear S^2_{max}, both within 3 km above the lapse rate tropopause.~~ Composite of the vertical wind shear for the 76 strong cyclones with $p_{msl,\,min} \leq 990$ hPa at the point in time of maximum intensity, averaged over the individual quasi-horizontal fields of maximum vertical wind shear S^2_{max} found within 3 km above the lapse rate tropopause for each cyclone. The black arrows indicate the orientation of the vertical cross-sections in Fig. 12.

Page 20 Figure 12 caption: Composites of flow features for the 76 strong cyclones with $p_{msl,\,min} \leq 990$ hPa at the point in time of maximum intensity. Vertical tropopause-based averaged cross-section composites, reaching from the cyclone centre (a) northwestward, (b) southwestward, (c) southeastward and (e) northeastward. Top row shows static stability N^2 and cloud ice water content as in Fig. 9, bottom row shows wind shear S^2 as in Fig. 10b. The orientation of the vertical cross-sections is indicated by the black arrows in Fig. 11.

Page 18 Line 9: ~~Figure 12 provides a strong indication that a co-location between the regions of enhanced static stability above the tropopause and the maximum in vertical shear of the horizontal wind exists. Figure 12a shows the quasi-horizontal composite of the maximum in wind shear within 3 km above the tropopause for the subset of strong cyclones ($p_{msl,\,min} \leq 990$ hPa). It reveals together with Fig. 7 that there is a co-location between the regions of maximum squared wind shear S^2_{max} above the tropopause and the regions of maximum enhancement in static stability N^2_{max} in the lower stratosphere. Figure 12 furthermore shows how both features are also vertically constrained north of the cyclone centre, resulting in the vertical overlap of the wind shear region and the TIL (see also Fig. 9 and Fig. 10b).~~

Figure 11 further illustrates the connection between the regions of enhanced static stability and the vertical shear of the horizontal wind in the vicinity of cyclones. It shows the composite derived from the quasi-horizontal fields of maximum wind shear S^2_{max} found within 3 km above the tropopause in the 76 strong cyclones. The region of largest mean wind shear matches with the region of maximum enhanced static stability (see Fig. 7b), with maximum values north and northeast of the cyclone centre within the wrapped-up ridge. The southern regions exhibit weaker mean wind shear, and the minimum values of S^2_{max} are located around the cyclone centre.

Figure 12 shows tropopause based averaged vertical cross-sections that cover the distance from the cyclone centre to the spherical cap radius of 15° and are oriented in different cardinal directions as indicated in Fig 11. These plots complement Fig. 10b and Fig. 11 and further confirm a co-location as well as a co-occurence of the regions of maximum wind shear S^2_{max} and the regions of maximum enhanced static stability N^2_{max}. They furthermore illustrate the validity and representativity of the composites derived from the individual quasi-horizontal fields. The quasi-horizontal composite in Fig. 7b strongly depends on the definition of the TIL-strength (in this case the maximum value of N^2 within 3 km above the tropopause), while the vertical cross-section composites in the top row of Fig. 12 solely depend on the tropopause definition (equivalently Fig. 11 and Fig. 12 bottom row for the vertical wind shear). However, both methods show a good agreement, aside from an overall shift of the absolute values as expected and described in Sect. 2.2.1.

Comment 6: Richardson number analysis: I find this very interesting. Do the corresponding plots for the case studies in section 3 show very low values of Ri above the tropopause (regions with $Ri < 1$)?

Reply to comment 6: The regions of enhanced static stability within the individual cyclones are mostly dominated by large vertical shear of the horizontal wind which results in low Richardson numbers despite the enhanced N^2, as is the case for the LC1 and LC2 case study (Figure R4). Several cyclones in our dataset exhibit regions with even very low Richardson numbers ($Ri < 1$) at tropopause altitudes, in anticyclonic upper tropospheric flow inside the ridge of the baroclinic waves and with partial overlap into the regions of enhanced static stability. These regions however appear as transient and localised features. A detailed analysis of such a case is subject to a corresponding study we are working on, which is in preparation to be submitted to ACPD.

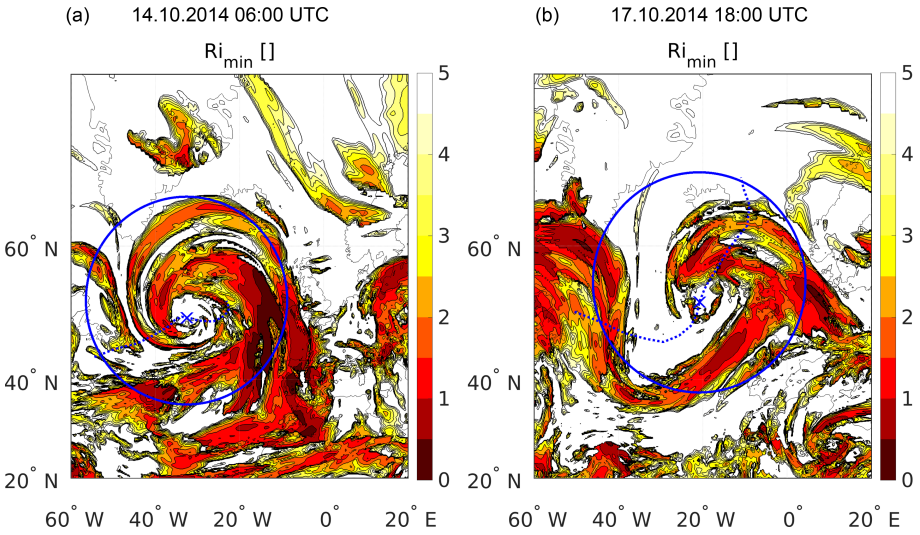

Figure R4. Minimum Richardson numbers Ri_{min} within 3 km above the thermal tropopause, at the point in time of maximum cyclone intensity a.) for the LC2 resembling baroclinic wave, and b.) for the LC1 resembling baroclinic wave.

Comment 7: P18 line 31. The Richardson numbers found are not low enough for turbulent flow. I would suggest not making such a strong statement in the conclusion.

Reply to comment 7: We rephrased the paragraph to make the statement less strong and to clarify that we do not expect the whole region to be dynamically unstable (because the Richardson numbers are still too large as you pointed out). We rather want to note that the general tendency towards high vertical wind shear in the region of interest (considering the variability of N^2 and S^2) points toward the possibility for localised turbulence.

Changes in the manuscript:

Page 21 Line 11: Mean Richardson numbers calculated for these flow conditions ~~favourable for turbulence~~ reveal a region of local minima in Ri right above the tropopause at around 5° north from the cyclone centre in the composite. ~~This result points toward a co-location between an enhancement in static stability above the tropopause and potential turbulent mixing of tropospheric and stratospheric air masses (Kunkel et al., 2016).~~ Taking into account the variability of N^2 and S^2 for individual cyclones, this result points toward the possibility of a co-location between enhanced static stability above the tropopause and

localised regions of turbulent mixing of tropospheric and stratospheric air masses (Kunkel et al., 2016).

Comment 8: The colour scale on some of the figures could be chosen to be slightly more intuitive. E.g., Fig 10 (c) At first glance, I thought the red values were bigger.

Reply to comment 8: We agree that this plot can be counterintuitive due to the inverted color scale, but we want to highlight the region with the tendency toward turbulent motion (i.e. low Richardson numbers) and therefore want to keep the inverted colors for this particular Figure. We added a note on this to the Figure caption. We furthermore changed the color scale to a lower maximum value to make the plot more easy to read.

Changes in the manuscript:

Page 18 Fig. 10 caption: Vertical tropopause-based averaged cross-section as in ~~Figure 8~~Fig. 9, but only north of the cyclone centre. Left panel: filled contours show mean vertical velocity, solid thin black line the $\omega = 0$ Pa s^{-1} isoline. Grey dashed lines are isolines of the cloud ice water content, steps as in Fig. 9. Middle panel: filled contour and solid black contour lines show squared vertical shear of horizontal wind S^2. Right panel: modified Richardson number mean Ri, with an inverted color scale (red represents low values) to highlight the tendency toward turbulent motion. ~~Grey~~Blue solid bold line in all three panels shows the $N^2_{mean} = 6 \times 10^{-4}$ s^{-2} isoline, dashed black lines the isentropes.

Other comments: P2, line 31. Fix reference - P4 line 3 "the a more", line 25 "oder" - P6 line 6, "North Africa an the" - P9 caption a) "seal level" - P12 line 7 "extend" - P13 lines 17 and 18 "This region of strong with..." Meaning unclear. - P14 line 8 "stronger" to more pronounced - P 16 fig 10 caption "Vertical crosssection as in figure 8" should be figure 9. also "north the cyclone", "of" missing.

Reply: We fixed the mistakes in the manuscript.

Point-by-point response to the second review

Comment 1: I found the introduction rather hard to read, with a lot of jargon that would be impenetrable to anyone new to the topic. I recommend reworking a lot of the language in the introduction section to make it clearer. For example, the 2nd paragraph on page 2 could be reworded.

Reply to comment 1: We agree that the introduction was written through the glasses of someone being rather familiar with the history of research on the topic of the tropopause inversion layer. We rephrased several formulations, reduced the technical description of numerical model experiment settings, and added descriptive caption-like sentences in between the paragraph to make the topic more approachable to someone who is less familiar with the phenomenon of the tropopause inversion layer. We however believe that some of the technical jargon is unavoidable when describing the approach and major outcome of the theoretical modelling studies on the TIL formation within baroclinic waves.

Changes in the manuscript:

Page 2 Line 7: This study focusses on the evolution of the TIL at midlatitudes, where the flow in the UTLS is largely dominated by baroclinic planetary and synoptic scale waves. ~~The role of such waves on the formation and maintenance of the TIL in midlatitudes has been the subject of a variety of scientific studies.~~ These waves play a major role concerning the formation and maintenance of the TIL in midlatitudes, and they have been subject of a variety of modelling studies on the TIL (Wirth, 2003, 2004; Wirth and Szabo, 2007; Erler and Wirth, 2011; Kunkel et al., 2014, 2016). ~~Idealised modelling studies showed that the TIL can be formed due to conservative dynamics. Wirth (2003, 2004) performed potential vorticity (PV) inversions on axisymmetric PV anomalies of different sign in an idealised background atmosphere, pointing out an adiabatic sharpening mechanism of the lower stratospheric temperature profile related to the convergence of the secondary circulation vertical wind in anticyclonic flow. They were furthermore able to show that the advection of enhanced static stability from low to high latitudes plays an important role for the lower stratospheric N^2 maximum in anticyclonic flow.~~ Wirth (2003, 2004) used idealised studies of frontogenesis to show how adiabatic flow can sharpen the static stability above the tropopause. The underlaying mechanisms are related to the convergence of the cross-frontal secondary circulation and to the advection of large N^2 values from low to high latitudes. ~~Wirth and Szabo (2007) performed baroclinic life cycle simulations with a comprehensive numerical weather prediction model and were able to confirm the concept of an adiabatic sharpening mechanism of the tropopause.~~ These studies were complemented by the work of Wirth and Szabo (2007) who confirmed the concept of an adiabatic sharpening mechanism of the tropopause in baroclinic life cycles using a comprehensive numerical weather prediction model. ~~Following up on these results, Erler and Wirth (2011) performed adiabatic baroclinic life cycle simulations with the same setup and concluded that breaking of baroclinic waves is an important process for the irreversible and permanent formation of a residual TIL as evident in the zonal or temporal mean states.~~ The nonlinear interactions during the breaking of synoptic scale waves are crucial for the appearance of a coherent background TIL in adiabatic flow, as shown by Erler and Wirth (2011). ~~Kunkel et al. (2014) performed similar baroclinic life cycle experiments with the focus on the impact of inertia-gravity waves on the thermal structure in the UTLS. They found that these waves, after being emitted from imbalances along the jet, modulate the ambient thermodynamic variables such as the static stability N^2 and persistently modify the TIL structure through the dissipation of the gravity waves.~~ Aside from adiabatic dynamics, diabatic processes have been shown to be of importance. Randel et al. (2007) showed that the radiative forcing of ozone and water vapour in the UTLS leads to a sharpening of the tropopause due to heating above and cooling below. Kunkel et al. (2016) extended the adiabatic simulations of baroclinic waves by including the contributions from different diabatic forcings. They showed that diabatic effects are important to maintain the TIL and that moist dynamic processes lead to the formation of small scale regions with large values of N^2. ~~The role of diabatic processes in the TIL formation during baroclinic life cycle simulations was then studied by the work of Kunkel et al., (2016), who attributed the relative to the adiabatic case stronger TIL evolution to diabatic processes related to moist dynamics and radiative effects of clouds reaching up to the tropopause.~~ Moreover, gravity waves emitted from instabilities along the jet can dissipate in the tropopause region, ultimately altering the thermal structure and thus the static stability N^2 (Kunkel et al., 2014). On larger scales the stratospheric residual circulation ~~also~~ furthermore contributes significantly to the sharpening of the tropopause (Birner, 2010) especially at midlatitudes and during winter, where the downwelling in the extratropics induces

a warming which lowers the tropopause and results in a strong localised positive forcing on the static stability. ~~Randel et al. (2007) performed radiative transfer model calculations to compare the radiative effect of realistic measurement-based mean ozone- and water vapour profiles to profiles with varying gradients of both constituents at tropopause height. They linked the strong gradients of ozone and water vapour at the tropopause to a dipole of the radiative forcing with cooling below and heating above the local tropopause. In turn this leads to an enhancement of static stability in the lower stratosphere.~~

The TIL in midlatitudes was furthermore studied using a combination of measurement and numerical weather prediction model data. Pilch Kedzierski et al. (2015) analysed the synoptic scale behaviour of the TIL based on Global Positioning System ~~(GPS-RO)~~ radio occultation (GPS-RO) temperature profiles in combination with data from the European Centre for Medium-Range Weather Forecasts (ECMWF). ~~They found the strongest TIL values in the midlatitudes within ridges and during winter, and thus confirmed and expanded previous more theoretical studies concerning the correlation between the TIL strength and the relative vorticity of the upper tropospheric flow.~~ They confirmed and expanded previous more theoretical studies that 1.) the strongest TIL in midlatitudes is found within ridges and during winter, and 2.) a strong correlation exists between the upper tropospheric relative vorticity and the strength of the TIL. Pilch Kedzierski et al. (2017) applied a wavenumber-frequency domain filtering method on GPS-RO temperature profiles and were able to attribute a major part of the instantaneous TIL signal in midlatitudes to the transient and reversible modulations caused by planetary- and synoptic-scale waves. In conclusion, these previous works show that the adiabatic dynamics of planetary and synoptic scale waves in the UTLS region along with diabatic processes and finally the wave breaking process play a major role ~~on one hand~~ concerning the instantaneous ~~and potentially reversible~~ sharpening of the lower stratospheric temperature gradients as well as ~~on the other hand~~ the formation of an irreversible and ~~permanent~~persistent ~~residual~~ background TIL.

~~The~~While previous studies either investigated the evolution of the TIL based on idealised model simulations, focussed on the zonal mean background TIL, or were based on satellite and radiosonde measurement data, the goal of this study is to complement these ~~previous studies~~approaches by analysing common structures of the TIL evolution in baroclinic waves over the North Atlantic in a spatially and temporally high resolution data set. Furthermore, we investigate the mean flow features within regions of enhanced static stability with a focus on the role of the TIL for cross-tropopause exchange, including a physical mechanism potentially leading to dynamical instabilities above the tropopause.

For this we use ECMWF operational analysis data over a five year period and first focus on the evolution of the TIL in individual life cycles.~~, and s~~Second we derive composites of life cycles to analyse common patterns in the evolution of the lower stratospheric static stability over a set of 130 individual baroclinic life cycles over the North Atlantic. The evaluation of ~~average~~mean atmospheric properties with composites, especially in the vicinity of cyclones was used in a variety of previous studies and based on a variety of underlying data. Wang and Rogers (2001) analysed dynamical and thermal characteristics of explosive cyclones during a 12 year period over the North Atlantic, based on ECMWF analysis data. Catto et al. (2010) compared composites of the 100 most intense extratropical cyclones in the northern hemisphere from the 40-year ECMWF reanalysis (ERA-40) data set and the high resolution global environment coupled climate model (HiGEM), to assess the capability of climate models to produce coherent airstream features~~, i.e. the warm conveyor belt, the cold conveyor belt and the dry intrusion~~. Recently, Flaounas et al. (2015) studied a set of 200 intensive Mediterranean cyclones based on a 20 year Weather Research and Forecasting (WRF) regional model data simulation with one focus among others on the UTLS PV forcing on the overall life cycle evolution and its synergy with the tropospheric development of the cyclones. To our knowledge the presented study is the first to focus on the TIL and ~~correlated~~associated features in the context of cyclone composites.

Comment 2: Also regarding the introduction, it could be made clearer exactly where the gaps lie that this paper seeks to address. At the bottom of page 1, "evidence for this relation still missing" implies that this paper will provide evidence, but I am unsure if this is a goal of the study. Some rewording might make the introduction clearer overall.

Reply to comment 2: After further consideration motivated by your comment we rephrased the paragraph in question to mitigate the implication on what the reader should expect from our analysis of the tropopause inversion layer. This change in combination with the changes made in the introduction section in reference to your first comment should clarify the major goals of this study.

We want to motivate the investigation of the role of the TIL concerning troposphere-stratosphere exchange processes. The TIL

is commonly regarded as a transport barrier, in agreement with the fluiddynamical ramifications of a layer of enhanced static stability. However, one key result of our study is the potential for cross-tropopause exchange in the late stage of a baroclinic life cycle. Our analysis for the special case of the regions of enhanced static stability in late stage extratropical baroclinic waves shows a superimposed tendency towards dynamic instability due to large vertical wind shear in these regions.

Changes in the manuscript:

Page 1 Line 23: ~~This co-location sometimes led to the assumption that the TIL might inhibit cross-tropopause transport (Hegglin et al., 2009; Gettelman and Wang, 2015), however, evidence for this relation is still missing.~~This co-location might imply a possible controlling function of the TIL for mixing in the UTLS, also based on the fluiddynamical ramifications of a layer of enhanced static stability, as large values of N^2 suppress vertical motion. Moreover, the TIL is essential for the vertical propagation of waves on different scales, ranging from small scale gravity waves to large scale Rossby waves (e.g., Birner, 2006; Sjoberg and Birner, 2014; Gisinger et al., 2017). The sharp jump in static stability at the tropopause from mean tropospheric values of $N^2 = 1 \times 10^{-4}\ \mathrm{s}^{-2}$ to mean stratospheric values of $N^2 = 4 \times 10^{-4}\ \mathrm{s}^{-2}$ or to the even larger values defining the TIL results in a maximum of the so called refractive index controlling the upward propagation of waves, and leading to partial or even total wave reflection at the tropopause. The overall role of the TIL concerning mixing processes between troposphere and stratosphere however is still not finally understood.

Page 3 Line 5: Furthermore, we investigate the mean flow features within regions of enhanced static stability with a focus on the role of the TIL for cross-tropopause exchange, including a physical mechanism potentially leading to dynamical instabilities above the tropopause.

Comment 3: Page 2 line 19: The "residual TIL" is mentioned more than once. Is it possible to define what this looks like?

Reply to comment 3: We reconsidered the formulation and changed the wording from "residual TIL" to "background TIL", which is more fitting and also more self-explanatory. The changes concern several sentences in the introduction section. The updated introduction with marked changes is already attached to our reply to your first comment.

Comment 4: Page 2 line 32: This Kedzierski et al reference is never returned to in the discussion section, although I am sure the results from the present paper confirm those results (the TIL strongest within the ridges).

Reply to comment 4: We describe the work by Pilch Kedzierski et al. (2015) in our introduction section because it gives a demonstrative measurement based description of the TIL in mid-latitudes. The study analyses hemispheric snapshots of the TIL distribution, as well as a statistical correlation analysis between the static stability above the tropopause and the upper tropospheric relative vorticity. We agree that the results from Pilch Kedzierski et al. (2015) match with our results concerning the synoptic scale variability of the TIL in mid-latitudes in ridges and troughs, but our analysis is specifically targeting late stage breaking baroclinic waves. Furthermore, we look at the shaping of the TIL in more detail than it would be possible from the global coverage rate of about 2000 daily GPS-RO profiles. We perceive the study of Pilch Kedzierski et al. (2015) as part of the basis for our work, where we try to expand their results by looking at the TIL evolution within troughs and ridges in a spatially and temporally higher resolved data set and describing the evolution. We added a reference to Pilch Kedzierski et al. (2015) in section 3.1 where we first describe the correlation between relative vorticity and static stability in troughs and ridges in our data set.

Changes in the manuscript:

Page 10 Line 1: This correlation especially holds true inside the 15° radius area and at the point in time of maximum cyclone intensity. This agrees well with the anticipated role of balanced dynamics (Wirth, 2003, 2004) and idealised baroclinic life cycle simulations with focus on the evolution of the TIL (e.g., Erler and Wirth, 2011). It furthermore agrees with the measurement based study by Pilch Kedzierski et al. (2015) concerning the correlation between the relative vorticity and the static

stability within troughs and ridges.

Comment 5: Page 3, line 33: L91 and L137 are not vertical resolutions, but the number of levels. Could you give more information about the actual vertical resolution here?

Reply to comment 5: We changed the formulation from vertical resolution to vertical level count. We furthermore added a description on the geometric vertical resolution in the UTLS, the region of interest in our study.

Changes in the manuscript:
Page 3 Line 31: We use six hourly available analysis fields during the given time period, with a grid spacing of 0.25°in the horizontal, a vertical ~~resolution~~level count of L91 for the years 2010 until 2012, and L137 for 2013 and 2014. The abbreviation L91/L137 describes the 91/137 vertical level of the IFS's native hybrid sigma coordinates ranging from the earth's surface up to 0.01 hPa atmospheric pressure, with corresponding level spacing of typically 300-400 m in the UTLS region.

Comment 6.: Page 6, line 16: Could you make clearer what is meant by a "lapse rate tropopause based vertical coordinate"? Also page 7, line 7: what is meant by "the absolute height coordinate is recovered by calculating the mean tropopause height at each horizontal location"?

Reply to comment 6: We replaced the expression "lapse rate tropopause based vertical coordinate" by a description of the method, and added a reference to another study (Birner, 2006) that describes the method in detail.
In reference to your second question, the composite of the cyclones is calculated in lapse rate tropopause based vertical coordinates. Each horizontal coordinate $(\Theta,\ \phi)$ of each cyclone within the new coordinate system still carries the information of the absolute tropopause height, therefore a mean tropopause height can be calculated and assigned at this location within the composite. Hereby the level zero in the lapse rate tropopause based coordinates is replaced by the mean tropopause height, and all other vertical levels present a certain distance from this mean tropopause height. We added this description to the manuscript.

Changes in the manuscript:
Page 7 Line 11: The original ECMWF IFS variables in latitude-longitude coordinates are ~~then~~ interpolated onto a ~~pillar~~column covered by the new coordinate system, ~~with a lapse rate tropopause based vertical coordinate and a vertical grid spacing of $\Delta z = 100$ m.~~with the vertical coordinate using the lapse rate based tropopause as reference altitude (Birner, 2006). The tropopause height is defined as zero with negative/positive height values below/above and a vertical grid spacing of $\Delta z = 100$ m.

Page 7 Line 16: The ensemble of tropopause based ~~pillars~~ columns of variables from each cyclone is then averaged to create a three-dimensional composite of the flow in the vicinity of the cyclones. Subsequently, the mean absolute height coordinate is recovered as follows. ~~by calculating the mean tropopause height at each horizontal location.~~ Each horizontal coordinate $(\Theta,\ \phi)$ of each individual cyclone within the new coordinate system still carries the information about the absolute tropopause height at that location, therefore a mean tropopause height can be calculated and assigned to that horizontal location within the composite.

Comment 7: Page 7, line 8: What is meant by "horizontal or quasi-horizontal variables"? Does this just mean the horizontal composites of particular variables?

Reply to comment 7: We rephrased the expression to "horizontal or quasi-horizontal fields". While the expression "horizontal fields" commonly refers to variables on a plane of uniform geometric height or sometimes uniform pressure level, we use the expression quasi-horizontal to describe two-dimensional fields that are distinctly not horizontally aligned as defined above, e.g. the TIL strength above the highly variable tropopause height (especially in the vicinity of cyclones). The expression

quasi-horizontal has been used in the same way in other studies (e.g., Wirth, 2003; Wirth and Szabo, 2007).

Changes in the manuscript:
Page 7 Line 22: In the special case of composites of horizontal or quasi-horizontal ~~variables~~fields like the potential vorticity on an isentropic surface or the TIL strength, we first calculate the fields for each cyclone and then afterwards the mean.

Comment 8: Page 8, line 11: Please do not start sentences with numerals.

Reply to comment 8: We wrote out the numeral.

Changes in the manuscript:
Page 8 Line 11: ~~24~~Twenty-four hours before the cyclone reaches maximum intensity the mean sea level pressure already falls below 975 hPa.

Comment 9: Figure 3: The dotted MSLP contour is hard to distinguish.

Reply to comment 9: We updated all contour plot showing the mean seal level pressure, as well as their description. The solid lines now depict mean sea level pressure isolines from 1013 hPa downwards in steps of 5 hPa, and the dashed lines still depict isolines of mean sea level pressure larger than 1013 hPa in 5 hPa steps.

Comment 10: Page 8, line 30: Is the maximum N^2 above the tropopause the best measure of TIL strength? It does seem to correlate well with the PV pattern, but would an average value give similar but smoother results? Have you tested this?

Reply to comment 10: The concern about which TIL strength definition is the most useful was also expressed by the other reviewer, and we gave a detailed explanation in our reply to that comment on why we chose the specific TIL-definition used in our study. We refer to the third comment in the first review and our answer to this comment. We prepared an additional set of plots of the TIL strength evolution for our case studies (LC1 and LC2, see Figures R1 and R2). These contour plots are based on a vertical average of N^2 as the TIL strength. They show a largely similar evolution of the TIL on a synoptic scale but a lot of fine scale variability is filtered due to the average. We prefer the maximum in N^2 as the TIL strength definition because we work with high resolution data and want to preserve the fine scale variability in our analysis. Furthermore, our definition of the TIL-strength is in accordance with previous studies (e.g., Erler and Wirth, 2011; Pilch Kedzierski et al., 2015). The validity of the TIL-strength definition we used is further confirmed by Fig. 12 which we added to the manuscript, on one hand as a response to comment 5 of the first review and on the other hand because it provides a better illustration of the issue that we tried to display in Fig. 11. We plotted a set of vertical tropopause-based cross-section composites similar to Figure 9 for different rotation angles around the cyclone centre. While these composites are only based on the lapse rate tropopause definition and not on the definition of the TIL-strength, they do agree very well with the composites of the maximum in N^2 above the tropopause from the individual cyclones. A description of this issue was also added to the manuscript as a response to comment 5 of the first review.

Comment 11: Figure 4: The caption seems to have incomplete sentences.

Reply to comment 11: We rephrased the caption, also due to the additional plot as a reply to comment 4 of the first review.

Changes in the manuscript:
Page 11 Figure 4 caption: Vertical cross-section over the North Atlantic on 14.10.2014 at ~~00:06 UTC and~~ 06:00 UTC, (a)

at 42° N and (b) at 60° N. The filled contour as well as the thin solid black contour lines show static stability N^2 in steps of 1×10^{-4} s^{-2}, dashed black lines show isentropes. The bold solid black line indicates the lapse rate tropopause, the dotted red line shows the 2 pvu isoline of potential vorticity.

Comment 12: Page 12, lines 9-10: I?m unsure of what this is referring to. Can you point out where the occlusion and the jet are located?

Reply to comment 12: After further consideration motivated by your comment, we prefer not to use the term occlusion for the case study of the cut-off cyclone, because this term commonly used in synoptic meteorology describes the seclusion of warm air from the ground due to the cold front moving faster than the warm front. The cyclone in question is migrating at rather low latitudes, therefore we find potential fronts to be less easy identified, and the description of the region of strongest TIL enhancement using the term occlusion (if justified) would still be confusing. We reworded the description, and added the 200 hPa wind maximum in Figure 6d (similar to Figure 3 and 5) to show the location of the jet (or jet streak).

Changes in the manuscript:
Page 13 Line 5: ~~The regions of high static stability above the tropopause are horizontally coherent with the occlusion as well as the region of outflow of ascending air masses into the jet.~~The regions of high static stability above the tropopause are located north of the cyclone centre inside the flow with negative relative vorticity, as well as inside the flow that turns anticyclonically north-west of the cyclone centre and towards the jet maximum (as indicated by the blue contour lines in Fig. 6d).

Comment 13: Page 12, lines 17-18: This sentence is unclear. Did those authors look at the same events?

Reply to comment 13: The authors of Erler and Wirth (2011) focused on the formation of the so called residual TIL during adiabatic baroclinic life cycle simulations, as is evident in their study for example in Hovmöller diagrams or averaged vertical profiles of N^2. They show snapshots of the evolution of the TIL strength as well (Figure 4), but they do not go into much detail on the connection with the surface cyclones. It is however possible to interpret the results of our study about when and where a strong TIL forms into the contour snapshots of N^2_{max} of their simulations, especially in combination with the information about the surface pressure given in their Figure 2. We agree that this note is very specific, but we want to keep it because we considered it notable in case a reader is further interested in a comparisson between our study and idealised baroclinic life cycle simluations.

Comment 14: Pages 15-16: With the discussion of the Richardson number, it would be useful to the reader to have an explanation of what the results really mean. On page 17, lines 7-9, it seems to imply that despite the low Ri, turbulent mixing may occur, whereas in the discussion section (p18, lines 32- 33) it seems to say that because of the low Ri turbulent mixing occurs. Please could you clarify this. In relation to this, are you suggesting that the strong TIL actually enhances the mixing across the tropopause? This would be in opposition to the Hegglin et al. (2009) and Gettelman and Wang (2015) references on page 1 of the introduction.

Reply to comment 14: We added a description of the Richardson number in Section 4, after the description of the maximum wind shear north of the cyclone centre within the region of enhanced N^2. This gives the reader a better introduction on how increased wind shear and co-located high static stability work towards a convectively stably stratified but dynamically unstable flow. We furthermore rephrased the first paragraph you quoted to resolve the contradiction you pointed out.
Your second question in comment 14 is closely related to your second comment in this review, and we already rephrased the paragraph in question motivated by the latter. The motivation for these changes is explained in our reply to comment 2. We do not want to imply that a strong TIL generally enhances mixing across the tropopause, because a layer of enhanced static stability can act as a transport barrier, on one hand because it inhibits vertical motion, and on the other hand (and related to the first

point) because it acts as a maximum of the refractive index controlling the upward propagation of atmospheric waves. For the specific case of the regions of enhanced static stability in late stage breaking baroclinic waves however we do see a tendency towards dynamic instability induced by vertical wind shear. The Richardson number with low values as an indicator for turbulent instability is composed of both constituents, $Ri = N^2\ S^{-2}$. When the wind shear component is of dominating order, this could result in a shallow (Whiteway et al., 2004) but systematic troposphere-stratosphere exchange process in this region, despite the enhanced static stability. This however is up to this point only hypothetical, because based on the analysis tools used in this study we can not estimate the efficiency of such an exchange process, therefore we only present the tendency towards maximum wind shear in regions of enhanced static stability without going into to much detail about possible consequences. We are currently working on a detailed analysis of a case study in reference to this topic, which is in preparation to be submitted to ACPD.

Changes in the manuscript:

Page 17 Line 5: Based on these results, we calculate the dimensionless gradient Richardson number Ri. It is defined as the ratio of static stability N^2 and the vertical shear of the horizontal wind S^2, $Ri = N^2 S^{-2}$. Enhanced values of N^2 describe a stably stratified flow with suppressed vertical motion, while enhanced vertical shear of the horizontal wind can result in dynamical shear instability. Linear wave theory predicts a critical Richardson number of $Ri_c = 0.25$, where dynamic instability can develop in stably stratified flow with $Ri < Ri_c$.

Page 17 Line 16: A second region of minimum mean Richardson numbers is located right above the tropopause near the cyclone centre, and extends into the regions of maximum static stability. In this region the vertical wind shear S^2 is the dominating factor that works towards dynamic instability.

Page 17 Line 33: ~~Richardson numbers of the order of 5-10 still represent a stable flow, but we want to stress that these are mean values from 76 cyclones, and based on vertical gradients of N^2 and S^2 derived from a vertical grid spacing of about $\Delta z \approx 300$ m.~~The lowermost stratosphere north of the cyclone centre exhibits Richardson numbers of $Ri = 5 - 10$ which are still well above the critical value of $Ri_c = 0.25$ for turbulent flow. These Richardson numbers however present an average of a highly non-linear measure over 76 cyclones. For individual cyclones Richardson numbers often exhibit much lower values in this region, eventually below the critical value Ri_c and thus are indicative for dynamic instability. Also we would like to remind the reader that these quantities are derived from model data with a vertical grid spacing of about $\Delta z \approx 300$ m. The two features of interest (N^2_{max} and S^2_{max}) typically exhibit a vertical extent of 1-3 km, therefore the model output profiles of N^2 and S^2 in the lowermost stratosphere can be expected to be a to a certain degree smoothed representation of the real atmosphere. A possible misrepresentation of the ratio between the two gradient-based measures N^2 and S^2 opens the possibility for an even larger range of Richardson numbers in the real flow. ~~Therefore~~In conclusion, there is the possibility that turbulence is present even in regions of enhanced static stability in the lower stratosphere which might affect cross tropopause transport in these regions.

Comment 15: Page 18, line 26: "strong tropospheric updrafts"... I wonder here if what you mean is the ascent associated with the warm conveyor belt (e.g. Madonna et al), which is where you would expect to see the diabatic heating. In Figure 3 it looks like the strongest TIL is clearly associated with the WCB at each time in the lifecycle. After the maximum intensity, the WCB anticyclonic outflow region (to the northeast of the cyclone) is the location of the strongest TIL. I think you need to include reference the WCB and how the observed features relate to it and the associated outflow. Ref: Madonna, E., H. Wernli, H. Joos, and O. Martius (2014a), Warm conveyor belts in the ERA-Interim dataset (1979? 2010). Part I: Climatology and potential vorticity evolution, J. Clim., 27, 3?26, doi:10.1175/JCLI-D- 12-00720.1.

Reply to comment 14: Thank you for pointing out this connection. While we did not use any tools like trajectory analysis to define and to investigate the warm conveyor belt, the apparent co-location of the WCB outflow and the regions of enhanced static stability is very notable, and has been pointed out before (Kunkel et al., 2016). We added a description of this issue throughout three different points in the manuscript; in the analysis Section of the LC2 case study, in the analysis of the vertical

cross-section composite of the ice water content and the vertical wind, and in the discussion Section.

Changes in the manuscript:

Page 10 Line 10: The regions of strongest enhancement of static stability above the tropopause in the second time step depicted in Fig. 3 as well as inside the deformed ridge in the third time step are associated to the regions commonly affected by the warm conveyor belt Madonna et al. (2014). The connection between the warm conveyor belt outflow and the regions of enhanced static stability above the tropopause is also a feature of the baroclinic life cycle simulations by Kunkel et al. (2016).

Page 16 Line 14: The ice clouds within and above the strong tropospheric updraft north of the cyclone centre reaching up to the tropopause with potential temperatures over $\Theta = 320$ K are features of the region where typically the warm conveyor belt outflow occurs (e.g., Madonna et al., 2014).

Page 21 Line 4: The regions of largest TIL enhancement are located north and northeast of the cyclone centre ~~above the occlusion and~~ above regions influenced by strong tropospheric updrafts and clouds reaching up to the tropopause, where in this central stage of the baroclinic life cycle typically the warm conveyor belt outflow occurs (e.g., Madonna et al., 2014; Kunkel et al., 2016). The high reaching clouds ~~This~~ indicate~~s~~ the importance of moist dynamical and radiative processes during the formation of the TIL (e.g., Randel et al., 2007; Kunkel et al., 2016).

References

Birner, T.: Fine-scale structure of the extratropical tropopause region, Journal of Geophysical Research Atmospheres, 111, 1–14, https://doi.org/10.1029/2005JD006301, 2006.

Birner, T.: Residual Circulation and Tropopause Structure, pp. 2582–2600, https://doi.org/10.1175/2010JAS3287.1, 2010.

Catto, J. L., Shaffrey, L. C., and Hodges, K. I.: Can climate models capture the structure of extratropical cyclones?, Journal of Climate, 23, 1621–1635, https://doi.org/10.1175/2009JCLI3318.1, 2010.

Erler, A. R. and Wirth, V.: The Static Stability of the Tropopause Region in Adiabatic Baroclinic Life Cycle Experiments, Journal of the Atmospheric Sciences, 68, 1178–1193, https://doi.org/10.1175/2010JAS3694.1, 2011.

Flaounas, E., Raveh-Rubin, S., Wernli, H., Drobinski, P., and Bastin, S.: The dynamical structure of intense Mediterranean cyclones, Climate Dynamics, 44, 2411–2427, https://doi.org/10.1007/s00382-014-2330-2, 2015.

Gettelman, A. and Wang, T.: Structural diagnostics of the tropopause inversion layer and its evolution, Journal of Geophysical Research Atmospheres, 120, 46–62, https://doi.org/10.1002/2014JD021846, 2015.

Gisinger, S., Dörnbrack, A., Matthias, V., Doyle, J. D., Eckermann, S. D., Ehard, B., Hoffmann, L., Kaifler, B., Kruse, C. G., Rapp, M., Gisinger, S., Dörnbrack, A., Matthias, V., Doyle, J. D., Eckermann, S. D., Ehard, B., Hoffmann, L., Kaifler, B., Kruse, C. G., and Rapp, M.: Atmospheric Conditions during the Deep Propagating Gravity Wave Experiment (DEEPWAVE), Monthly Weather Review, 145, 4249–4275, https://doi.org/10.1175/MWR-D-16-0435.1, 2017.

Hanley, J. and Caballero, R.: Objective identification and tracking of multicentre cyclones in the ERA-Interim reanalysis dataset, Quarterly Journal of the Royal Meteorological Society, 138, 612–625, https://doi.org/10.1002/qj.948, 2012.

Hegglin, M. I., Boone, C. D., Manney, G. L., and Walker, K. A.: A global view of the extratropical tropopause transition layer from Atmospheric Chemistry Experiment Fourier Transform Spectrometer O3, H2O, and CO, Journal of Geophysical Research Atmospheres, 114, 1–18, https://doi.org/10.1029/2008JD009984, 2009.

Kunkel, D., Hoor, P., and Wirth, V.: Can inertia-gravity waves persistently alter the tropopause inversion layer?, Geophysical Research Letters, 41, 7822–7829, https://doi.org/10.1002/2014GL061970, 2014.

Kunkel, D., Hoor, P., and Wirth, V.: The tropopause inversion layer in baroclinic life-cycle experiments: The role of diabatic processes, Atmospheric Chemistry and Physics, 16, 541–560, https://doi.org/10.5194/acp-16-541-2016, 2016.

Madonna, E., Wernli, H., Joos, H., and Martius, O.: Warm conveyor belts in the ERA-Interim Dataset (1979-2010). Part I: Climatology and potential vorticity evolution, Journal of Climate, 27, 3–26, https://doi.org/10.1175/JCLI-D-12-00720.1, 2014.

Pilch Kedzierski, R., Matthes, K., and Bumke, K.: Synoptic-scale behavior of the extratropical tropopause inversion layer, Geophysical Research Letters, 42, 10 018–10 026, https://doi.org/10.1002/2015GL066409, 2015.

Pilch Kedzierski, R., Matthes, K., and Bumke, K.: Wave modulation of the extratropical tropopause inversion layer, Atmospheric Chemistry and Physics, 17, 4093–4114, https://doi.org/10.5194/acp-17-4093-2017, 2017.

Randel, W. J., Wu, F., and Forster, P.: The Extratropical Tropopause Inversion Layer: Global Observations with GPS Data, and a Radiative Forcing Mechanism, Journal of the Atmospheric Sciences, 64, 4489–4496, https://doi.org/10.1175/2007JAS2412.1, 2007.

Sjoberg, J. P. and Birner, T.: Stratospheric Wave–Mean Flow Feedbacks and Sudden Stratospheric Warmings in a Simple Model Forced by Upward Wave Activity Flux, Journal of the Atmospheric Sciences, 71, 4055–4071, https://doi.org/10.1175/JAS-D-14-0113.1, 2014.

Wang, C.-C. and Rogers, J. C.: A Composite Study of Explosive Cyclogenesis in Different Sectors of the North Atlantic. Part I: Cyclone Structure and Evolution, Monthly Weather Review, 129, 1481–1499, https://doi.org/10.1175/1520-0493(2001)129<1481:ACSOEC>2.0.CO;2, 2001.

Whiteway, J. A., Klaassen, G. P., Bradshaw, N. G., and Hacker, J.: Transition to turbulence in shear above the tropopause, Geophysical Research Letters, 31, 2–5, https://doi.org/10.1029/2003GL018509, 2004.

Wirth, V.: Static Stability in the Extratropical Tropopause Region, Journal of the Atmospheric Sciences, 60, 1395–1409, https://doi.org/10.1175/1520-0469(2003)060<1395:SSITET>2.0.CO;2, 2003.

Wirth, V.: A dynamical mechanism for tropopause sharpening, Meteorologische Zeitschrift, 13, 477–484, https://doi.org/10.1127/0941-2948/2004/0013-0477, 2004.

Wirth, V. and Szabo, T.: Sharpness of the extratropical tropopause in baroclinic life cycle experiments, Geophysical Research Letters, 34, 10–13, https://doi.org/10.1029/2006GL028369, 2007.

Composite analysis of the tropopause inversion layer in extratropical baroclinic waves

Thorsten Kaluza[1], Daniel Kunkel[1], and Peter Hoor[1]

[1]Institute for Atmospheric Physics, Johannes-Gutenberg University Mainz, Mainz, Germany

Correspondence: Thorsten Kaluza (kaluzat@uni-mainz.de)

Abstract. The variability and similarities in the evolution of the tropopause inversion (TIL) layer during cyclongenesis in the North Atlantic storm track are investigated using operational meteorological analysis data (Integrated Forecast System from the European Centre for Medium-Range Weather Forecasts). For this a total amount of 130 cyclones have been analysed which evolved during the months August through October between $2010 - 2014$ over the North Atlantic. Their paths of migration along with associated flow features in the upper troposphere / lower stratosphere (UTLS) have been tracked using the mean sea level pressure. Subsets of the 130 cyclones have been used for composite analysis using minimum sea level pressure to filter the cyclones based on their strength.

The composite structure of the TIL strength distribution in connection with the overall UTLS flow strongly resembles the structure of the individual cyclones. Key results are that a strong dipole in tropopause inversion layer strength forms in regions of cyclonic wrap-up of UTLS air masses of different origin and isentropic potential vorticity. These air masses are associated with the cyclonic rotation of the underlaying cyclones. The maximum values of enhanced static stability above the tropopause occur north and northeast of the cyclone centre, vertically aligned with outflow regions of strong updraft and cloud formation up to the tropopause, which are situated in anticyclonic flow patterns in the upper troposphere. These regions are colocated with a maximum of vertical shear of the horizontal wind. The strong wind shear within the TIL results in a local minimum of Richardson numbers, representing the possibility for turbulent instability and potential mixing (or air mass exchange) within regions of enhanced static stability in the lowermost stratosphere.

1 Introduction

The tropopause inversion layer (TIL) is a ubiquitous feature of the upper troposphere/lower stratosphere (UTLS) region in equatorial, midlatitude, and polar regions (e.g., Birner et al., 2002; Gettelman and Wang, 2015). It is commonly defined as a vertically confined layer of enhanced static stability and is usually analysed using the squared Brunt Väisälä frequency, $N^2 = g\Theta^{-1}\partial_z\Theta$ (Birner et al., 2002). In the extratropics, the TIL is co-located to a region of strong trace gas gradients between the troposphere and the stratosphere (Hegglin et al., 2009; Kunz et al., 2009; Schmidt et al., 2010), which define the extratropical transition layer (Ex-TL, Pan et al. (2004); Hegglin et al. (2009)), or mixing layer (Hoor et al., 2002, 2004). ~~This co-location sometimes led to the assumption that the TIL might inhibit cross-tropopause transport (Hegglin et al., 2009; Gettelman and Wang, 2015), however, evidence for this relation is still missing.~~This co-location might imply a possible con-

trolling function of the TIL for mixing in the UTLS, also based on the fluiddynamical ramifications of a layer of enhanced static stability, as large values of N^2 suppress vertical motion. Moreover, the TIL is essential for the vertical propagation of waves on different scales, ranging from small scale gravity waves to large scale Rossby waves (e.g., Birner, 2006; Sjoberg and Birner, 2014; Gisinger et al., 2017). The sharp jump in static stability at the tropopause from mean tropospheric values of $N^2 = 1 \times 10^{-4}$ s^{-2} to mean stratospheric values of $N^2 = 4 \times 10^{-4}$ s^{-2} or to the even larger values defining the TIL results in a maximum of the so called refractive index controlling the upward propagation of waves, and leading to partial or even total wave reflection at the tropopause. The overall role of the TIL concerning mixing processes between troposphere and stratosphere however is still not finally understood.

This study focusses on the evolution of the TIL at midlatitudes, where the flow in the UTLS is largely dominated by baroclinic planetary and synoptic scale waves. ~~The role of such waves on the formation and maintenance of the TIL in midlatitudes has been the subject of a variety of scientific studies.~~ These waves play a major role concerning the formation and maintenance of the TIL in midlatitudes, and they have been subject of a variety of modelling studies on the TIL (Wirth, 2003, 2004; Wirth and Szabo, 2007; Erler and Wirth, 2011; Kunkel et al., 2014, 2016). ~~Idealised modelling studies showed that the TIL can be formed due to conservative dynamics. Wirth (2003, 2004) performed potential vorticity (PV) inversions on axisymmetric PV anomalies of different sign in an idealised background atmosphere, pointing out an adiabatic sharpening mechanism of the lower stratospheric temperature profile related to the convergence of the secondary circulation vertical wind in anticyclonic flow. They were furthermore able to show that the advection of enhanced static stability from low to high latitudes plays an important role for the lower stratospheric N^2 maximum in anticyclonic flow.~~ Wirth (2003, 2004) used idealised studies of frontogenesis to show how adiabatic flow can sharpen the static stability above the tropopause. The underlaying mechanisms are related to the convergence of the cross-frontal secondary circulation and to the advection of large N^2 values from low to high latitudes. ~~Wirth and Szabo (2007) performed baroclinic life cycle simulations with a comprehensive numerical weather prediction model and were able to confirm the concept of an adiabatic sharpening mechanism of the tropopause.~~ These studies were complemented by the work of Wirth and Szabo (2007) who confirmed the concept of an adiabatic sharpening mechanism of the tropopause in baroclinic life cycles using a comprehensive numerical weather prediction model. ~~Following up on these results, Erler and Wirth (2011) performed adiabatic baroclinic life cycle simulations with the same setup and concluded that breaking of baroclinic waves is an important process for the irreversible and permanent formation of a residual TIL as evident in the zonal or temporal mean states.~~ The nonlinear interactions during the breaking of synoptic scale waves are crucial for the appearance of a coherent background TIL in adiabatic flow, as shown by Erler and Wirth (2011). ~~Kunkel et al. (2014) performed similar baroclinic life cycle experiments with the focus on the impact of inertia-gravity waves on the thermal structure in the UTLS. They found that these waves, after being emitted from imbalances along the jet, modulate the ambient thermodynamic variables such as the static stability N^2 and persistently modify the TIL structure through the dissipation of the gravity waves.~~ Aside from adiabatic dynamics, diabatic processes have been shown to be of importance. Randel et al. (2007) showed that the radiative forcing of ozone and water vapour in the UTLS leads to a sharpening of the tropopause due to heating above and cooling below. Kunkel et al. (2016) extended the adiabatic simulations of baroclinic waves by including the contributions from different diabatic forcings. They showed that diabatic effects are important to maintain the TIL and that moist dynamic pro-

cesses lead to the formation of small scale regions with large values of N^2. ~~The role of diabatic processes in the TIL formation during baroclinic life cycle simulations was then studied by the work of Kunkel et al., (2016), who attributed the relative to the adiabatic case stronger TIL evolution to diabatic processes related to moist dynamics and radiative effects of clouds reaching up to the tropopause.~~ Moreover, gravity waves emitted from instabilities along the jet can dissipate in the tropopause region, ultimately altering the thermal structure and thus the static stability N^2 (Kunkel et al., 2014). On larger scales the stratospheric residual circulation ~~also~~ furthermore contributes significantly to the sharpening of the tropopause (Birner, 2010) especially at midlatitudes and during winter, where the downwelling in the extratropics induces a warming which lowers the tropopause and results in a strong localised positive forcing on the static stability. ~~Randel et al. (2007) performed radiative transfer model calculations to compare the radiative effect of realistic measurement-based mean ozone- and water vapour profiles to profiles with varying gradients of both constituents at tropopause height. They linked the strong gradients of ozone and water vapour at the tropopause to a dipole of the radiative forcing with cooling below and heating above the local tropopause. In turn this leads to an enhancement of static stability in the lower stratosphere.~~

The TIL in midlatitudes was furthermore studied using a combination of measurement and numerical weather prediction model data. Pilch Kedzierski et al. (2015) analysed the synoptic scale behaviour of the TIL based on Global Positioning System ~~(GPS-RO)~~ radio occultation (GPS-RO) temperature profiles in combination with data from the European Centre for Medium-Range Weather Forecasts (ECMWF). ~~They found the strongest TIL values in the midlatitudes within ridges and during winter, and thus confirmed and expanded previous more theoretical studies concerning the correlation between the TIL strength and the relative vorticity of the upper tropospheric flow.~~ They confirmed and expanded previous more theoretical studies that 1.) the strongest TIL in midlatitudes is found within ridges and during winter, and 2.) a strong correlation exists between the upper tropospheric relative vorticity and the strength of the TIL. Pilch Kedzierski et al. (2017) applied a wavenumber-frequency domain filtering method on GPS-RO temperature profiles and were able to attribute a major part of the instantaneous TIL signal in midlatitudes to the transient and reversible modulations caused by planetary- and synoptic-scale waves. In conclusion, these previous works show that the adiabatic dynamics of planetary and synoptic scale waves in the UTLS region along with diabatic processes and finally the wave breaking process play a major role ~~on one hand~~ concerning the instantaneous ~~and potentially reversible~~ sharpening of the lower stratospheric temperature gradients as well as ~~on the other hand~~ the formation of an irreversible and ~~permanent~~persistent ~~residual~~ background TIL.

~~The~~While previous studies either investigated the evolution of the TIL based on idealised model simulations, focussed on the zonal mean background TIL, or were based on satellite and radiosonde measurement data, the goal of this study is to complement these ~~previous studies~~approaches by analysing common structures of the TIL evolution in baroclinic waves over the North Atlantic in a spatially and temporally high resolution data set. Furthermore, we investigate the mean flow features within regions of enhanced static stability with a focus on the role of the TIL for cross-tropopause exchange, including a physical mechanism potentially leading to dynamical instabilities above the tropopause.

For this we use ECMWF operational analysis data over a five year period and first focus on the evolution of the TIL in individual life cycles.~~, and s~~Second we derive composites of life cycles to analyse common patterns in the evolution of the lower stratospheric static stability over a set of 130 individual baroclinic life cycles over the North Atlantic. The evaluation of

~~average~~mean atmospheric properties with composites, especially in the vicinity of cyclones was used in a variety of previous studies and based on a variety of underlying data. Wang and Rogers (2001) analysed dynamical and thermal characteristics of explosive cyclones during a 12 year period over the North Atlantic, based on ECMWF analysis data. Catto et al. (2010) compared composites of the 100 most intense extratropical cyclones in the northern hemisphere from the 40-year ECMWF reanalysis (ERA-40) data set and the high resolution global environment coupled climate model (HiGEM), to assess the capability of climate models to produce coherent airstream features~~, i.e. the warm conveyor belt, the cold conveyor belt and the dry intrusion~~. Recently, Flaounas et al. (2015) studied a set of 200 intensive Mediterranean cyclones based on a 20 year Weather Research and Forecasting (WRF) regional model data simulation with one focus among others on the UTLS PV forcing on the overall life cycle evolution and its synergy with the tropospheric development of the cyclones. To our knowledge the presented study is the first to focus on the TIL and ~~correlated~~associated features in the context of cyclone composites.

The paper is structured as follows. In Sect. 2 we present the data set, the surface cyclone tracking algorithm and our approach to derive composites of different dynamical and thermodynamical variables in the UTLS. In Sect. 3 we illustrate the evolution of the UTLS features for two different life cycles which remarkably resemble the well known life cycles LC1 and LC2 from Thorncroft et al. (1993). In Sect. 4 we present composites of a variety of variables from different subsets of the cyclones emphasising the evolution of the TIL in baroclinic life cycles as well as associated flow features. We close our discussion in Sect. 5 by summarising our findings and putting them into perspective of previous studies.

2 Data and methods

2.1 ECMWF operational analysis data

For the detection of cyclone tracks we use operational analysis fields from the integrated forecast system (IFS) from the European Centre for Medium-Range Weather Forecasts (ECMWF), for August to October from 2010 until 2014. The spatial extent of the area covers the North Atlantic from 60° W to 20° E and from 20° N to 75° N, and therefore encompasses the autumn maximum of Atlantic storm tracks (Wernli and Schwierz, 2006). We use six hourly available analysis fields during the given time period, with a grid spacing of 0.25° in the horizontal, a vertical ~~resolution~~level count of L91 for the years 2010 until 2012, and L137 for 2013 and 2014. The abbreviation L91/L137 describes the 91/137 vertical level of the IFS's native hybrid sigma coordinates ranging from the earth's surface up to 0.01 hPa atmospheric pressure, with corresponding level spacing of typically $300-400$ m in the UTLS region. Moreover, the choice of the time period as well as the region of the data was motivated by the preparation of the airborne measurement campaign WISE (Wave driven isentropic exchange) which took place over the North Atlantic in autumn 2017.

We decided to use the operational analysis data over e.g. ~~the~~ a more consistent reanalysis data set like ERA-Interim, due to the finer vertical resolution in the tropopause region. While ERA-Interim with 60 model levels has a vertical grid spacing of about 1 km in the UTLS, the operational analysis has a vertical grid spacing of about $300-400$ m, depending on the tropopause location and on the vertical grid spacing of L91 and of L137. In particular, this leads to a much better representation of the static stability in the lower stratosphere. The formation of the TIL in numerical models is known to be sensitive to the horizontal and

vertical resolution as well as their ratio (e.g., Birner, 2006; Wirth and Szabo, 2007; Son and Polvani, 2007; Erler and Wirth, 2011).

We use analysis data on model levels which provides the best vertical resolution in the UTLS of roughly 300 m. Many of the desired variables such as the temperature T, the three-dimensional wind (u, v, ω), the cloud ice water content $ciwc$ and relative vorticity ζ_{rel} are directly provided by the ECMWF, while other quantities have to be derived from the primary fields, such as static stability N^2, potential vorticity PV, vertical wind shear S^2, and the Richardson number Ri.

We define the strength of the TIL as the maximum in static stability within 3 km above the lapse rate tropopause. The lapse rate tropopause is defined as the lowest level where the temperature lapse rate falls below $2.0\ \mathrm{K\ km^{-1}}$ and its average between this level and all higher levels within 2 km above this level remains below this value (WMO, 1957). We ~~do this~~ use this specific TIL strength definition, since the high resolution data shows large variability in the UTLS region, with often several maxima evident above the tropopause. Therefore, we find this definition of the TIL strength to be preferable over e.g. the first maximum in static stability above a threshold ($4\times10^{-4}\ \mathrm{s^{-2}}$, e.g., Gettelman and Wang, 2015). Another way to describe the static stability above the tropopause is to calculate the mean value of N^2 over a predefined vertical extent relative to the tropopause (e.g., Kunkel et al., 2014). While such a TIL strength definition achieves very similar results on a synoptic scale to the ones we will describe in Sect. 3, it also filters a lot of small scale variability and therefore partly neutralises the advantage of analysing high resolution data.

2.2 Cyclone tracking

A major goal of this study is to analyse the evolution of dynamical features in the UTLS in life cycles of baroclinic waves, and link these with the evolution of the static stability N^2 above the tropopause. Baroclinic life cycles up to the point of breaking are often associated with surface cyclones (e.g., Thorncroft et al., 1993), and the flow in the UTLS above these cyclones is an important region in regard to the enhancement in static stability above the tropopause. Several methods are available to trace cyclones, using e.g. the associated maximum in relative vorticity on lower ~~oder~~ or middle tropospheric pressure levels, or the minimum in mean sea level (MSL) pressure. The IMILAST experiment (Neu et al., 2013) showed that many of these methods achieve comparable results. We tested several methods with short time periods and with comparable results. Ultimately, we decided to use the sea level pressure field due to the smoothness of this field compared to e.g. the relative vorticity, which makes it easier to identify cyclone centres. Our algorithm therefore identifies surface cyclones in the MSL pressure field and traces them in time and space.

The tracking algorithm is based on Hanley and Caballero (2012), and searches local minima in the MSL pressure field. Since our data has a fine horizontal grid spacing and is limited to the North Atlantic, we had to partly adapt the tracking algorithm to our data set. The major steps are 1.) smoothing of the MSL pressure field, 2.) identification of all local minima at all time steps, and 3.) the connection of the local minima from consecutive time steps to cyclone tracks. The following paragraph will give more details.

A local minimum in a gridded MSL pressure field is defined as a grid point having a lower value than its surrounding 8 grid points. To reduce the amount of local MSL pressure minima found at each time step, a Cressman filter (Cressman, 1959) is

applied, averaging each grid point in the field with its neighbouring grid points within a radius $r < r_0$ (r_0 being 500 km), using weights of $(r_0^2 - r^2)/(r_0^2 + r^2)$. The smoothed field exhibits less local minima, reducing the amount of criteria needed to define a cyclone center, without altering the tracks of the cyclones fundamentally. After applying the Cressman filter and following once more Hanley and Caballero (2012), the MSL pressure field at each time step is projected onto an area-preserving Lambert projection centred at the North Pole, to counteract the bias in zonal resolution caused by the convergence of the meridians on the native latitude-longitude-grid. The projected MSL pressure field is then interpolated onto a regular equidistant grid with 28 km grid spacing, which corresponds to the 0.25° horizontal resolution at the equator. The algorithm now searches and saves every local minimum in the MSL pressure field, with two extra criteria being applied: 1.) an upper threshold of $p_t = 1007.25$ hPa, and 2.) the neglection of all minima located over orography higher than 1500 m. The first criterium replaces the pressure gradient criterium applied in Hanley and Caballero (2012), since the limitation to a regional domain makes it difficult to calculate consistent pressure gradients. The value for p_t was determined by testing several values below 1013.25 hPa, with 1007.25 hPa being the largest value of minimum MSL pressure where our algorithm was able to connect the local minima to coherent cyclone tracks. Our algorithm therefore neglects very weak minima in the pressure field, but since weak cyclones or cyclones in very early/very late stages of their life cycles are often not strongly connected to the upper tropospheric flow, it is sufficient for this study to track them not from their very first nor until their very last appearance. Also we are focussing on the time periods around the mature stage of the baroclinic waves, i.e. when the MSL pressure reaches its lowest values. The second criterion is another result of the IMILAST experiment (Neu et al., 2013) and is applied due to the error associated with reducing the surface level pressure to sea level from such altitudes.

In the next step the algorithm connects minima from consecutive time steps by searching in a given radius for the nearest minimum. For minima associated with a new formed cyclone the search radius in the second time step is 720 km from the position where the cyclone first appears. For minima already existing for two or more time steps the algorithm follows Wernli and Schwierz (2006) with a 'first guess' approach, where the first guess location of the cyclone is a linear continuation of the track in latitude-longitude-coordinates: $\mathbf{x}^*(t_{n+1}) = \mathbf{x}(t_n) + 0.75[\mathbf{x}(t_n) - \mathbf{x}(t_{n-1})]$. Wernli and Schwierz (2006) introduce the factor of 0.75 because cyclone movement tends to get slower during a cyclone's life cycle. The corresponding MSL pressure minimum is then defined as the nearest minimum from $\mathbf{x}^*(t_{n+1})$ within a radius of 840 km. For more information concerning the values of the search radii and the first guess approach see Hanley and Caballero (2012) and Wernli and Schwierz (2006). Following yet another result from the IMILAST experiment (Neu et al., 2013) only cyclones with a lifetime of at least 24 hours are further considered which translates to at least five 6-hourly time steps in the IFS analysis data. The algorithm furthermore neglects cyclones with less than two time steps before and/or after the global minimum in MSL pressure along their path to make sure that the actual intensification period is covered by the data. We want to emphasize that due to these two criteria only extratropical cyclones are selected. Tropical cyclones in extratropical transition emerging from the western edge of our data region which might have a strong signal in the MSL field but no real intensification period are neglected by the algorithm. Figure 1 shows the cyclone paths tracked by the algorithm after applying all criteria. The distribution of tracks matches well with the climatological cyclone frequencies described in Wernli and Schwierz (2006). Aside from the large accumulation over the North Atlantic there are also several tracks located over North Africa and the Mediterranean Sea. The relatively small

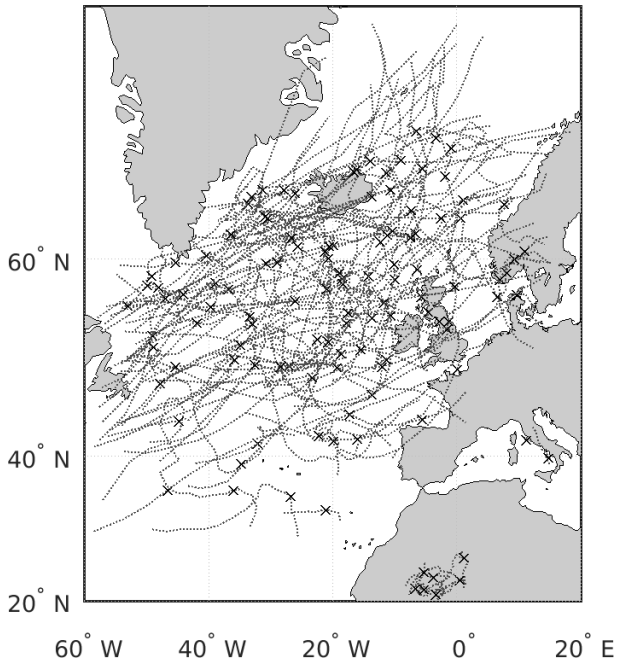

Figure 1. Mercator projection of the area covered, with all 139 cyclone tracks found by the algorithm. Crosses indicate the location of minimum sea level pressure along each track.

number of tracks over the Mediterranean Sea can be explained by the $p_t = 1007.25$ hPa upper limit criterium, and the fact that these Mediterranean cyclones hardly exhibit strong minima in the MSL pressure field. This study focusses on Atlantic storm tracks, therefore the cyclones over North Africa and the Mediterranean Sea are sorted out by a geographical criterium.

2.2.1 Composites of extratropical cyclones

Ultimately, we want to analyse the variability of the tropopause inversion layer within extratropical baroclinic waves. For this, we compute composites of the cyclones at the time of maximum intensity which we define as the occurrence of the global minimum surface pressure along the track. We select a subset of the gridded data as provided by the ECMWF for each cyclone by rotating the pole of a spheric polar coordinate system $(\Theta,\ \phi)$ onto the centre of the cyclone and interpolated the original data onto that new grid. The horizontal resolution of the new coordinate system is set to $0.25°$ and the spherical cap radius to $\Theta_{max} = 15°$ ~~(Fig. 2)~~. The radius is chosen such that all relevant features around the cyclone centre are covered. Figure 2 illustrates the interpolation of the data from the original latitude-longitude grid provided by the ECMWF (light grey area for the whole sphere, dark grey for the limited area used in this study) onto an arbitrarily placed new spherical polar coordinate system (orange area). The rotation of the new coordinate system onto the cyclone centre is performed following Bengtsson

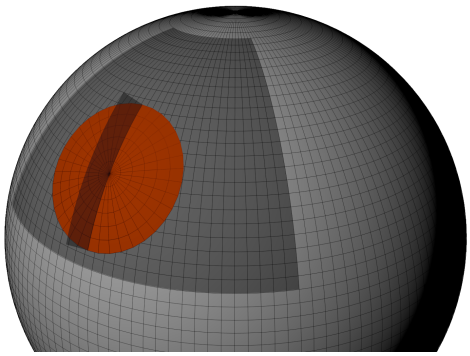

Figure 2. Schematic of the size of the analysed region (dark grey) in comparison to the full sphere, as well as the size of a rotated spheric polar coordinate system (orange) with $\Theta_{max} = 15^{\circ}$ radius. The dark grey semi-transperent upright plane illustrates (with exaggerated vertical extent) the vertical cross-section aligned from north to south as displayed in Fig. 9.

et al. (2007), who provide a detailed description of the rotation matrix in their appendix. The original ECMWF IFS variables in latitude-longitude coordinates are ~~then~~ interpolated onto a ~~pillar~~column covered by the new coordinate system, ~~with a lapse rate tropopause based vertical coordinate and a vertical grid spacing of $\Delta z = 100$ m.~~with the vertical coordinate using the lapse rate based tropopause as reference altitude (Birner, 2006). The tropopause height is defined as zero with negative/positive height values below/above and a vertical grid spacing of $\Delta z = 100$ m. The interpolation onto the new coordinate system based on the centre of the surface cyclone does not account for a potential vertical tilt of the cyclone. However since this study focusses on the point in time of maximum cyclone intensity when the vertical structure tends to align, we find a tilt to be negligible. The ensemble of tropopause based ~~pillars~~ columns of variables from each cyclone is then averaged to create a three-dimensional composite of the flow in the vicinity of the cyclones. Subsequently, the mean absolute height coordinate is recovered as follows. ~~by calculating the mean tropopause height at each horizontal location.~~ Each horizontal coordinate $(\Theta,\ \phi)$ of each individual cyclone within the new coordinate system still carries the information about the absolute tropopause height at that location, therefore a mean tropopause height can be calculated and assigned to that horizontal location within the composite.

In the special case of composites of horizontal or quasi-horizontal ~~variables~~fields like the potential vorticity on an isentropic surface or the TIL strength, we first calculate the fields for each cyclone and then afterwards the mean. This method preserves more information because the three-dimensional tropopause based averaging still smoothes vertical information due to the variability of e.g. the height of the maximum in N^2 above the tropopause. In contrast to other studies analysing cyclone composites (e.g., Bengtsson et al., 2007; Catto et al., 2010), we keep the orientation of each individual cyclone instead of rotating them dependent on their path of migration. In our case this approach leads to a better representation of the dynamical and thermodynamical features in the UTLS.

3 The lower stratospheric static stability evolution during two baroclinic wave breaking events

Before we present the result of the cyclone composite, we first discuss two cases of individual cyclones and associated TIL evolution over the North Atlantic. We choose these cases since both cyclones are associated with upper tropospheric baroclinic wave breaking events very similar to the ones described in idealised baroclinic life cycle simulations. The first case study shows an evolution comparable to an LC2 (life cycle 2), while the second one exhibits distinct features of an LC1 (life cycle 1) wave breaking event (Thorncroft et al., 1993). Although the waves occur consecutively in time and space, they are not interacting directly and the cyclones at surface level evolve relatively isolated from each other, in contrast to multi-cyclone-centres as described for example by Hanley and Caballero (2012).

3.1 Baroclinic wave with LC2 characteristics

Figure 3 shows three consecutive time steps of the evolution of the first baroclinic wave with the time of maximum intensity depicted in the second row. We focus our analysis and discussion on the flow features inside the 15° radius around the cyclone centre. Furthermore, we focus our discussion on sea level pressure, isentropic potential vorticity (IPV) at 330 K, strength of the tropopause inversion layer as defined in the beginning of Sect. 2, and relative vorticity at the lapse rate tropopause (from left to right in Fig. 3).

~~24~~Twenty-four hours before the cyclone reaches maximum intensity the mean sea level pressure already falls below 975 hPa. The IPV shows a baroclinic wave centred above the tracked surface cyclone centre, with large IPV values coming from high latitudes and tilting in northwest-southeast direction into the jet. During the intensification of the surface cyclone the upper air wave enters what Thorncroft et al. (1993) call the cyclonic wrap-up phase which in this case study exhibits distinct features of an LC2. During the wrap-up which is vertically aligned with the strong surface cyclone the trough stays on the northern cyclonic shear side of the jet streak as indicated by the 200 hPa horizontal wind maximum in Fig. 3d. The wave breaking event is meridionally confined by the jet streak and only a very thin streamer of enhanced IPV air turns anticyclonically on the last day depicted in Fig. 3. The relative vorticity at lapse rate tropopause height correlates with the IPV where cyclonic (anticyclonic) flow exhibits large (low) values of IPV. The regions with relatively small (large) values of IPV and anticyclonic (cyclonic) flow exhibit enhanced (reduced) values of static stability above the tropopause. This correlation especially holds true inside the 15° radius area and at the point in time of maximum cyclone intensity. This agrees well with the anticipated role of balanced dynamics (Wirth, 2003, 2004) and idealised baroclinic life cycle simulations with focus on the evolution of the TIL (e.g., Erler and Wirth, 2011). It furthermore agrees with the measurement based study by Pilch Kedzierski et al. (2015) concerning the correlation between the relative vorticity and the static stability within troughs and ridges. The regions with the largest values of static stability up to $N^2 = 10 \times 10^{-4}$ s^{-2} are located inside the ridge in the first time step and later in the second time step in the tropospheric IPV air mass which is wrapped up around the underlaying cyclone centre. In the last time step the TIL strength especially within the 15° radius reverts to lower values. We want to highlight the fact that the enhancement of the TIL strength during the wave breaking event is not uniform, but rather shows a large spatial variability and

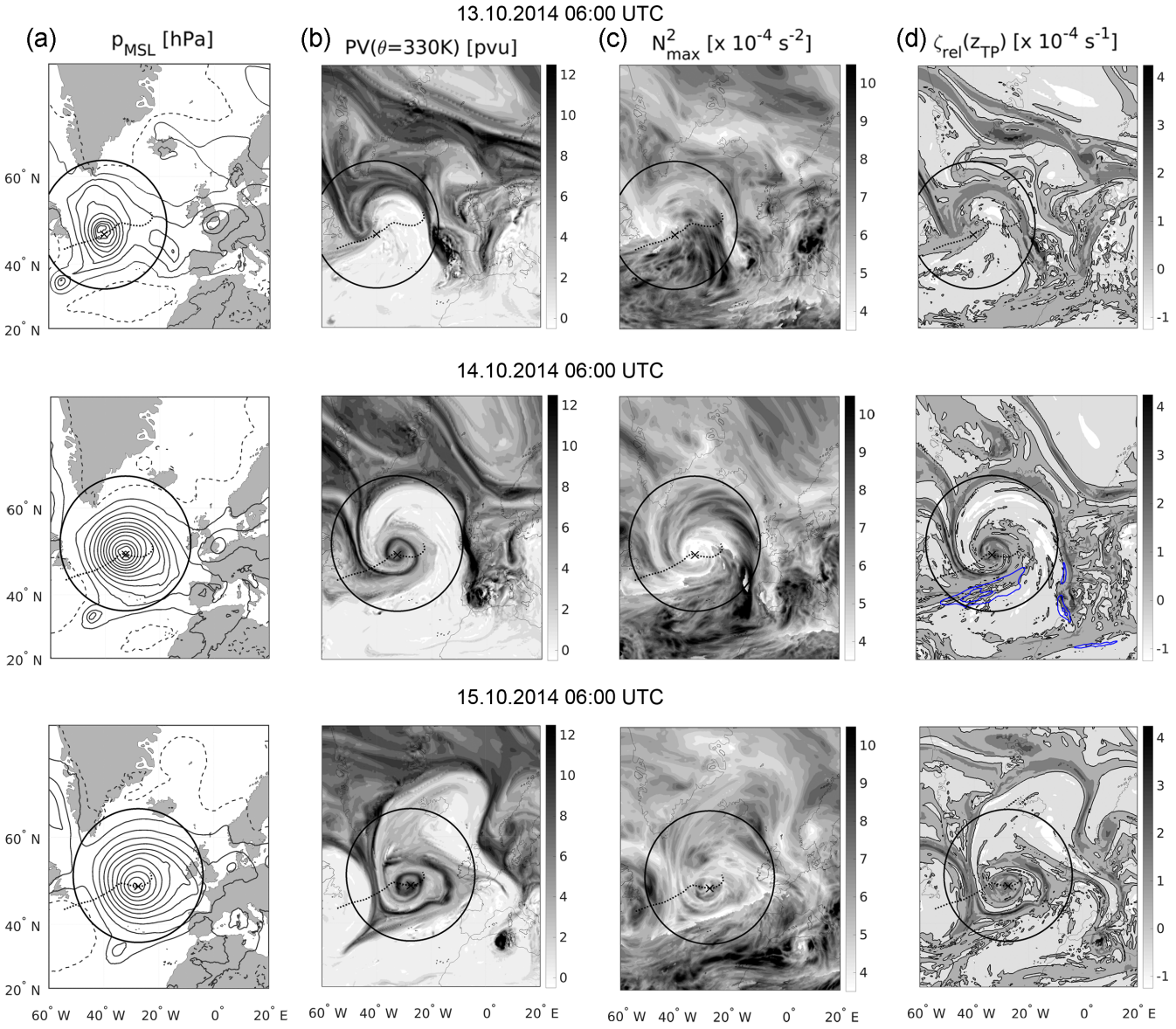

Figure 3. Evolution of a baroclinic wave breaking event as seen in ECMWF IFS analysis data. The middle row represents the 14th of October 2014 at 06:00 UTC~~,~~ (the point in time of maximum cyclone intensity), the upper and lower row show the situation 24 hours prior and past the maximum intensity. Column (a) shows the pressure at mean ~~seal~~ sea level ~~(solid lines $p_{msl} < 1013$ hPa, dashed $p_{msl} > 1013$ hPa, dotted $p_{msl} = 1013$ hPa)~~(solid lines $p_{msl} \leq 1013$ hPa, dashed lines $p_{msl} > 1013$ hPa, in steps of 5 hPa), (b) the IPV on 330 K, (c) the maximum of static static stability N^2_{max} within 3 km above the thermal tropopause as indicator for the TIL strength, and (d) the relative vorticity at lapse rate tropopause height. Blue lines in middle row show 40 and 50 $\mathrm{m\ s^{-1}}$ horizontal windspeed isolines at 200 hPa. Dashed black line shows the path of migration of the tracked cyclone, with the position of the cyclone centre at the point in time of the meteorological field displayed marked by the black x. Black circles show the 15° radius used for the composites. Note the deformation of the circles due to the mercator projection.

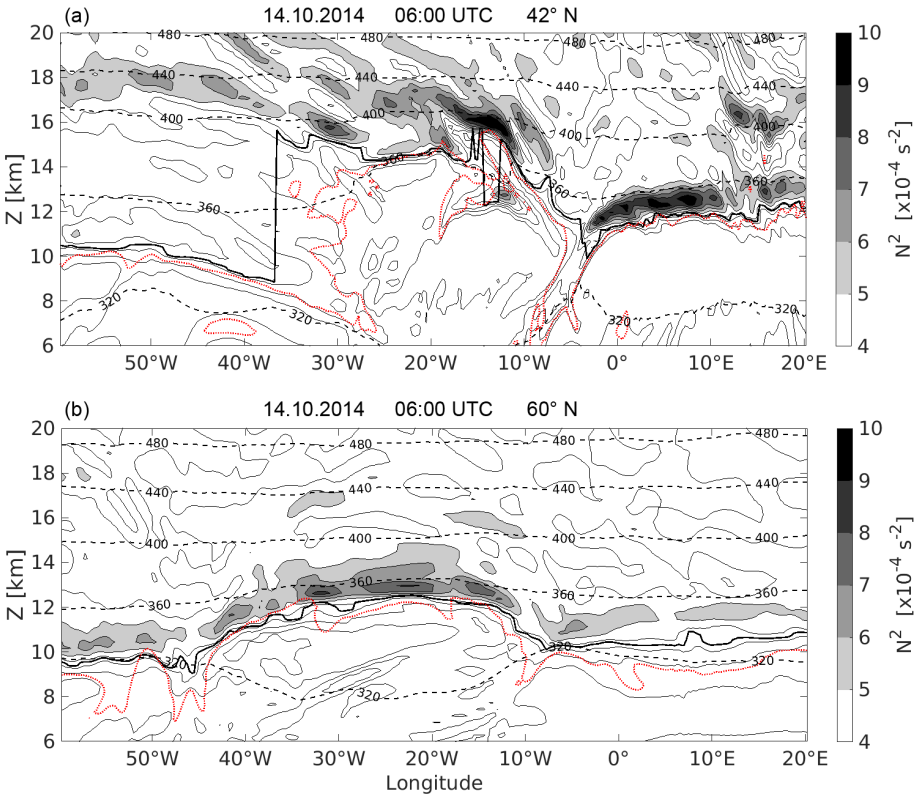

Figure 4. Vertical cross-section over the North Atlantic on 14.10.2014 at ~~00:06 UTC and~~ 06:00 UTC, (a) at 42° N and (b) at 60° N. The filled contour as well as the thin solid black contour lines show static stability N^2 in steps of 1×10^{-4} s^{-2}, dashed black lines show isentropes. The bold solid black line indicates the lapse rate tropopause, the dotted red line shows the 2 pvu isoline of potential vorticity.

wave-like patterns on different horizontal scales. The regions of strongest enhancement of static stability above the tropopause in the second time step depicted in Fig. 3 as well as inside the deformed ridge in the third time step are associated to the regions commonly affected by the warm conveyor belt Madonna et al. (2014). The connection between the warm conveyor belt outflow and the regions of enhanced static stability above the tropopause is also a feature of the baroclinic life cycle simulations by Kunkel et al. (2016).

The TIL strength at lower latitudes in the quasi-horizontal illustration (Fig. 3c) sometimes exhibits strong gradients or jumps which appear non-coherent. These strong gradients are sort of an evaluation artefact, due to 1.) the restriction of the TIL strength to the global maximum in static stability within 3 km above the lapse rate tropopause, 2.) the high variability of the tropopause defining lapse rate in the high resolution data, 3.) the occurrence of sharp tropopause jumps and double tropopauses (especially during wave breaking events), and 4.) the strongly structured TIL itself. The occurence of such features should be kept in mind when analysing such synoptic situations in a high resolution data set. We compared such prominent structures in the quasi horizontal illustration of the TIL with a variety of vertical cross-sections, to ensure that the statements we make

about the TIL evolution hold true and are in fact not a numerical evaluation artefact. Figure 4a shows an example for a vertical cross-section corresponding to the second time step depicted in Fig. 3 and at 42° N. It illustrates the large variability of the three dependent variables PV, static stability N^2 and the lapse rate tropopause height. The jump of the lapse rate tropopause at about 37° W as well as the small scale stratospheric PV intrusion at about 12° W illustrate the complexity of the tropopause location and the challenge to account for this by the different definitions of the tropopause and the TIL.

The vertical cross-section in Fig. 4b shows the TIL structures at 60° N on the same day and north of the cyclone centre. It illustrates that the regions of enhanced static stability exhibit less variability at this latitude. They are located above the ridge between 40° W and 10° W, with the wave-like horizontal pattern that is also visible in Fig. 3c.

3.2 Baroclinic wave with LC1 characteristics

Figure 5 shows the subsequent baroclinic wave breaking event 3 days later over the North Atlantic. The mean sea level pressure on 16 October still shows two distinct minima, the decaying northern one associated with the previous wave breaking event, as well as a newly formed minimum. The background state of the UTLS is still significantly distorted due to wave breaking event of the LC2 described in Sect. 3.1. Similar to the previous case a relatively small scale baroclinic wave is evident in the IPV field above the underlaying surface cyclone centre. In contrast to the previous case, as the surface cyclone grows stronger and the upper air wave enters the wrap-up phase (Fig. 5 middle row), the initially cyclonically tilted trough with enhanced values of IPV turns anticyclonically and later on a substantial part of the trough penetrates the jet in its excursion southwards. The jet splits into two jet streaks (middle row Fig. 5d) and the trough gets thinned, eventually producing a cut-off (Fig. 6). These wave breaking characteristics meet the definition of an LC1 as described by Thorncroft et al. (1993). During the evolution of the cyclone the relations between tropospheric IPV, anticyclonic relative vorticity at tropopause height, and an enhancement in static stability above the tropopause are all evident. The regions of maximum static stability with values up to $N^2 = 10 \times 10^{-4}$ s^{-2} are again located inside the ridge of low IPV air wrapping up around the underlaying cyclone centre about the time of maximum cyclone intensity. The thinning and southward moving trough itself exhibits low values of static stability N^2 above the tropopause, in agreement with its positive relative vorticity, but the flow around the trough shows no distinct strong signal in the quasi-horizontal static stability distribution, especially when compared to the cyclonic wrap-up 24 hours earlier.

Figure 6 shows a comparable evolution about two days later for the secondary cyclone associated with the cut-off which formed from the thinning streamer. This cyclone was also tracked by the algorithm and while it is weaker and exhibits less horizontal ~~extend~~ extent than the two previous cases, the region of maximum static stability with values of up to $N^2 = 10 \times 10^{-4}$ s^{-2} still evolves inside the wrapped up low-IPV air. The wrapped up cut-off exhibits maximum static stability values of about $N^2 = 4 \times 10^{-4}$ s^{-2}. ~~The regions of high static stability above the tropopause are horizontally coherent with the occlusion as well as the region of outflow of ascending air masses into the jet.~~The regions of high static stability above the tropopause are located north of the cyclone centre inside the flow with negative relative vorticity, as well as inside the flow that turns anticyclonically north-west of the cyclone centre and towards the jet maximum (as indicated by the blue contour lines in Fig. 6d).

In conclusion, we analysed two subsequent baroclinic life cycles, the first resembling an LC2, and the second an LC1 when

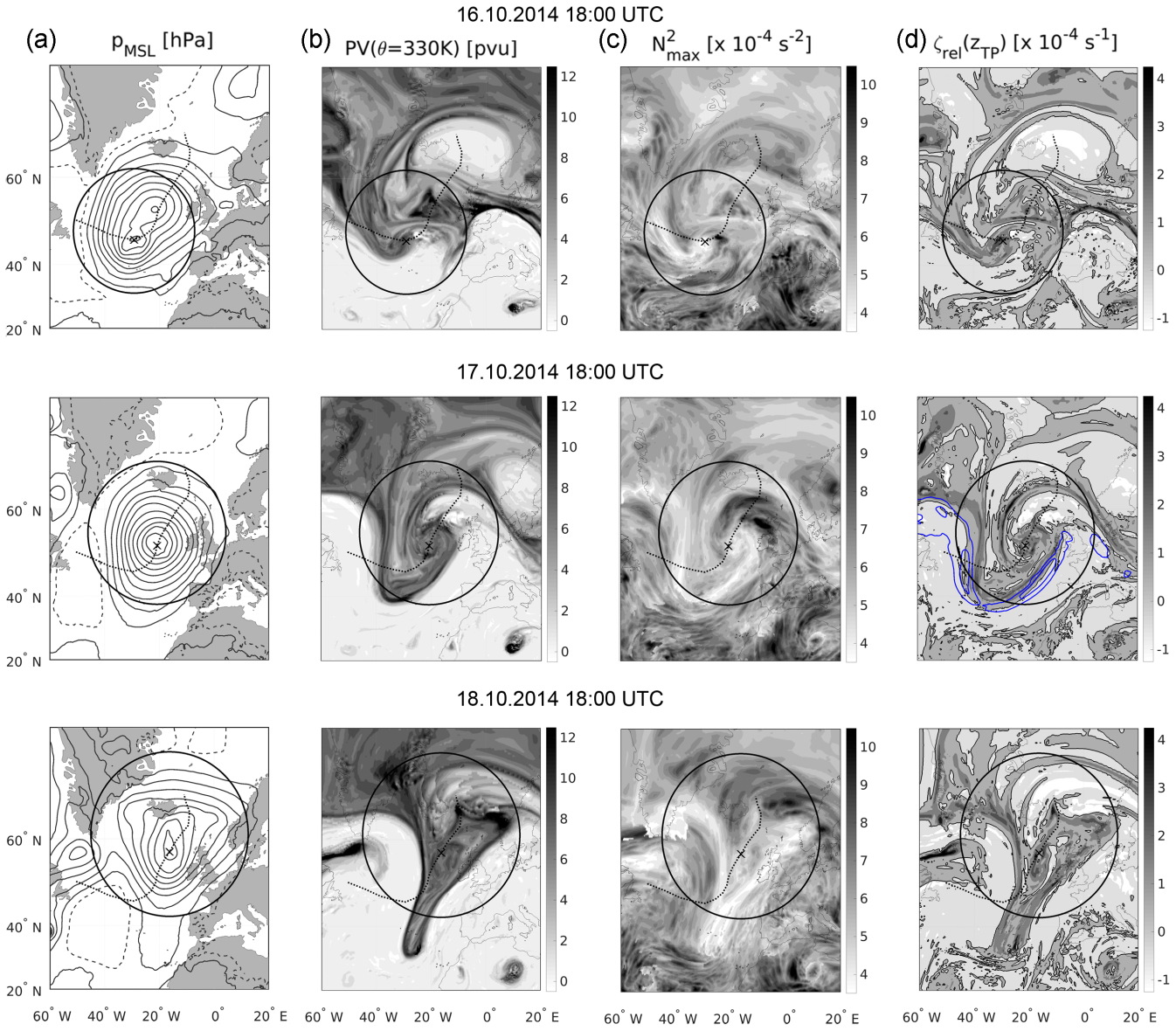

Figure 5. As in Fig. 3, but for the subsequent cyclone with maximum intensity on 17 October 2014 at 18:00 UTC, depicted in the middle row. Top row 24 hours earlier respectively bottom row 24 hours later.

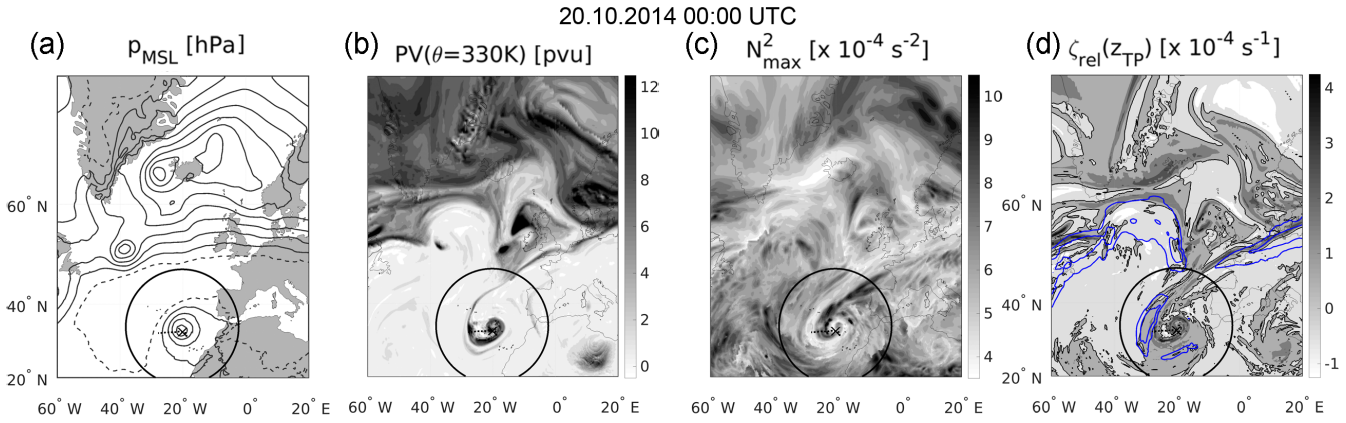

Figure 6. As in Fig. 3, but only for one point in time, showing the tracked cyclone associated with the upper tropospheric cut-off from the previous baroclinic wave breaking.

compared with idealised baroclinic life cycle simulations. In both cases the regions of strongest enhancement in static stability above the tropopause are located inside the ridge of low-IPV air moving northward from low latitudes and wrapping up around the underlaying primary cyclone about the time of maximum cyclone intensity. The flow around the southward excursion of the trough in the LC1 wave exhibits no distinct signal, until a secondary cyclone associated with the cut-off from the trough evolves. This *cyclone-linked* behaviour can also be seen in the idealised baroclinic life cycle simulations from Erler and Wirth (2011). Their Figure 4 shows a comparable evolution of the TIL strength with consideration that there are two northern surface cyclone intensification periods and one cut-off related cyclone forming at low latitudes.

Based on the analysis of these two case studies, we further motivate the analysis of the evolution of the TIL during baroclinic life cycles based on the flow above surface cyclones. We recognise that surface cyclones exist which are not linked to baroclinic wave breaking events and also baroclinic wave breaking events (in the sense of meridional irreversible redistribution of isentropic potential vorticity) exist which are not linked to surface cyclones. Nevertheless, we expect a composite of strong surface cyclones to give a characteristic representation of the flow where a strong TIL forms during the subset of those baroclinic wave breaking events which are in fact linked to surface cyclones.

4 Composite analysis of extratropical cyclones over the North Atlantic

In the following section we present composites of upper tropospheric / lower stratospheric flow features to define a mean characteristic evolution of the flow features in the UTLS above surface cyclones during baroclinic wave breaking events. We compute composites of subsets of the tracked cyclones based on the surface cyclone strength, because we expect the strength to be a good indicator for the amount of coupling between the surface cyclone and the flow in the UTLS. We abstain from

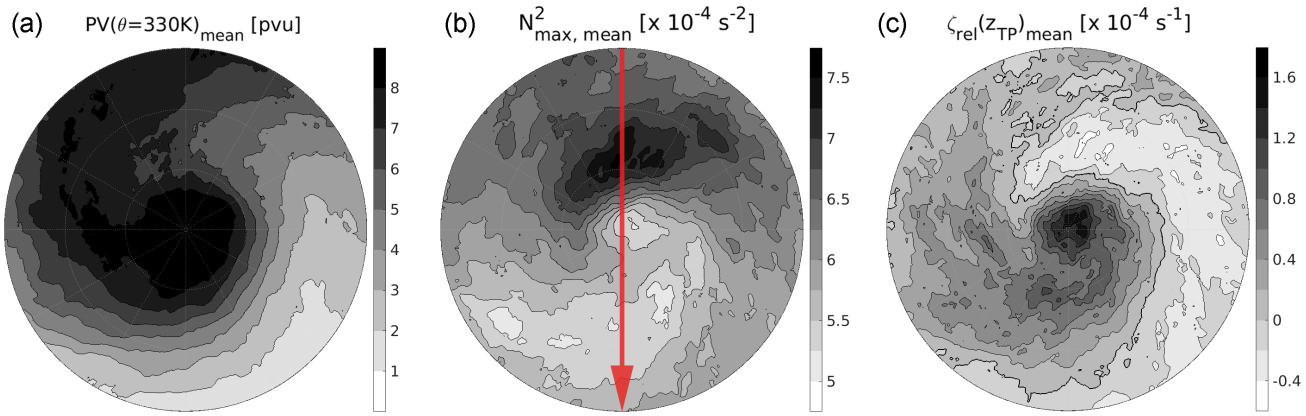

Figure 7. Composite of flow features for the 76 strong cyclones with $p_{msl,\ min} \leq 990$ hPa at the point in time of maximum intensity. From left to right, IPV on 330 K, TIL strength N^2_{max}, and relative vorticity ζ_{rel} at lapse rate tropopause height. The $\zeta_{rel} = 0\ \ \mathrm{s}^{-1}$ isoline is indicated by the black solid line. The red arrow in the middle indicates the orientation of the cross-section in Fig. 9.

presenting composites from cyclone subsets based on other criteria because the amount of cyclones tracked in our data set quickly reduces to a statistically non-significant amount when specific criteria are applied.

Figure 7 shows the quasi-horizontal composites of selected features from the 76 strong cyclones with $p_{msl,\ min} \leq 990$ hPa. The three contour plots show a mean state of the UTLS flow which is in its basic features comparable to the ones discussed in the two case studies of baroclinic wave breaking events. The first contour plot shows a streamer of stratospheric IPV on 330 K reaching from north-west into the cyclone centre, with a cyclonic rotational component. Naturally, the lowest values of IPV are located in the south and gradually approach the IPV values of the stratospheric streamer when rotating counterclockwise around the cyclone centre along the wrap-up. This region of strong ~~with respect to the cyclone centre~~ tangential gradients of IPV (with respect to the cyclone centre) exhibits to large parts a negative mean relative vorticity at tropopause height and also large values of static stability in the lower stratosphere. The maximum values of static stability are located north of the cyclone centre with maximum values up to $N^2_{max,\ mean} = 7.5 \times 10^{-4}\ \mathrm{s}^{-2}$. The stratospheric IPV streamer as well as the southern regions of strong radial IPV gradients exhibit a cyclonic relative vorticity at tropopause height as well as a relatively weak TIL with values of about $N^2_{max,\ mean} \approx (5 - 5.5) \times 10^{-4}\ \mathrm{s}^{-2}$.

In Fig. 8 the same contour plots are displayed for a subset of very strong cyclones as well as a subset of weak cyclones. The composites in the top row represent the 30 very strong cyclones with $p_{msl,\ min} \leq 980$ hPa. The dominating cyclonic rotational component is ~~stronger~~ more pronounced and the air masses with distinctly different features are wrapped up around the cyclone centre to a larger degree. The relative vorticity and the TIL strength still correlate well and their horizontal gradients are sharper compared to those in Fig. 7. The latter is not caused by a stronger TIL in case of $p_{msl,\ min} \leq 980$ hPa, but more due to a clearer

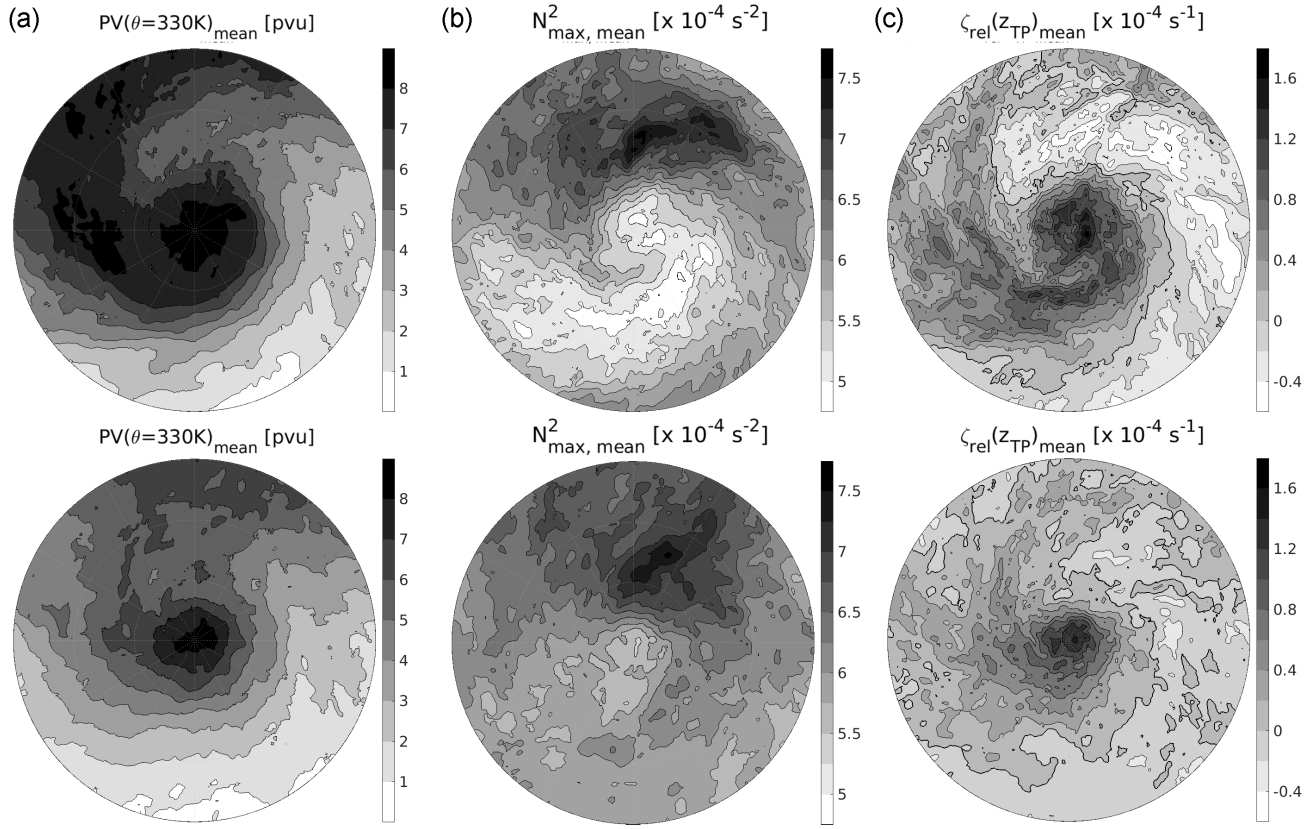

Figure 8. As in Fig. 7, but for 1.) top row: for the 30 very strong cyclones with $p_{msl,\ min} \leq 980$ hPa, and 2.) bottom row: the 54 weak cyclones with $p_{msl,\ min} > 990$ hPa.

separation and also a significant decrease in TIL strength in the cyclonic flow.

The 54 weak cyclones with $p_{msl,\ min} > 990$ hPa are presented in the bottom row of Fig. 8. The features described for the subsets of the strong and the very strong cyclones are still evident, however, with smoother gradients in all three features depicted and a weaker separation between tropospheric and stratospheric (influenced) air masses. The region of maximum enhancement of static stability above the tropopause is still located north of the cyclone centre and also still reaches mean values of about $N^2_{max,\ mean} \approx (7 - 7.5) \times 10^{-4}\ \mathrm{s}^{-2}$.

Figure 9 shows a mean vertical cross-section from north to south through the cyclone centre for the 76 strong cyclones with $p_{msl,\ min} \leq 990$ hPa along the red line as indicated in Fig. 7. The thermal and dynamical tropopauses ~~have~~ both exhibit minimum height in the cyclone centre and both slope upward south of the cyclone centre. Furthermore, the regions of maximum TIL strength partly align vertically above regions of ascending air and cloud formation in the troposphere indicated by the

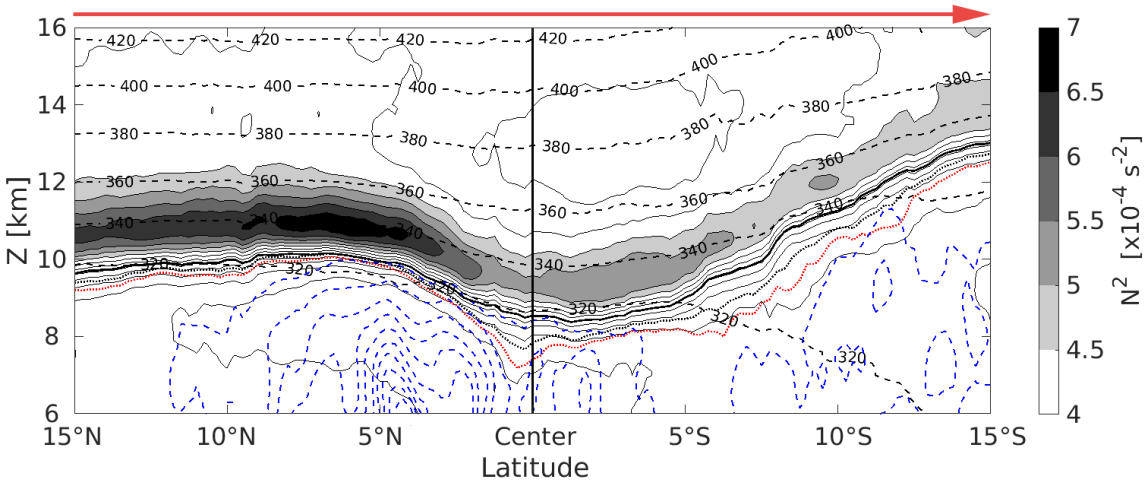

Figure 9. Vertical cross-section of the mean state from the 76 strong cyclones, from north to south through the centre of the cyclone, as indicated by the red arrow here and in Fig. 7b. The cross-section is composed of the tropopause based mean of vertical profiles at each latitude. The mean tropopause height has been restored. Filled contour as well as solid black contour lines show static stability N^2 in steps of 0.5×10^{-4} s^{-2}, dashed black lines isentropes, and dashed blue lines the cloud ice water content (ciwc) with the first isoline at and steps of 5×10^{-6} kg/kg. The bold solid black line indicates the lapse rate tropopause, the dotted red (black) line the 2 pvu (2.5 pvu) isoline of potential vorticity, indicating near-tropopause PV gradients.

cloud ice water reaching up to the lapse rate tropopause. This hints towards the role of moist dynamical processes in the formation of the TIL (Kunkel et al., 2016). To analyse the region of strongest enhancement in static stability north of the cyclone centre in more detail we derive the composites shown in Fig. 10. Depicted are the vertical wind, the squared vertical shear of the horizontal wind S^2, and the gradient Richardson number similar to the northern half of the cross-section in Fig. 9 and for the same subset of cyclones ($p_{msl,\,min} \leq 990$ hPa). The mean vertical wind ω correlates well with the mean cloud ice water content. The ice clouds within and above the strong tropospheric updraft north of the cyclone centre reaching up to the tropopause with potential temperatures over $\Theta = 320$ K are features of the region where typically the warm conveyor belt outflow occurs (e.g., Madonna et al., 2014). The stratosphere shows no distinct mean vertical velocity signal and the troposphere far north from the cyclone centre exhibits slowly descending air masses. The squared vertical shear of the horizontal wind speed $S^2 = (\partial u/\partial z)^2 + (\partial v/\partial z)^2$ shows a maximum above the tropopause, with a remarkable overlap into the regions of maximum static stability. Based on these results, we calculate the dimensionless gradient Richardson number Ri. It is defined as the ratio of static stability N^2 and the vertical shear of the horizontal wind S^2, $Ri = N^2 S^{-2}$. Enhanced values of N^2 describe a stably stratified flow with suppressed vertical motion, while enhanced vertical shear of the horizontal wind can result in dynamical shear instability. Linear wave theory predicts a critical Richardson number of $Ri_c = 0.25$, where dynamic instability can

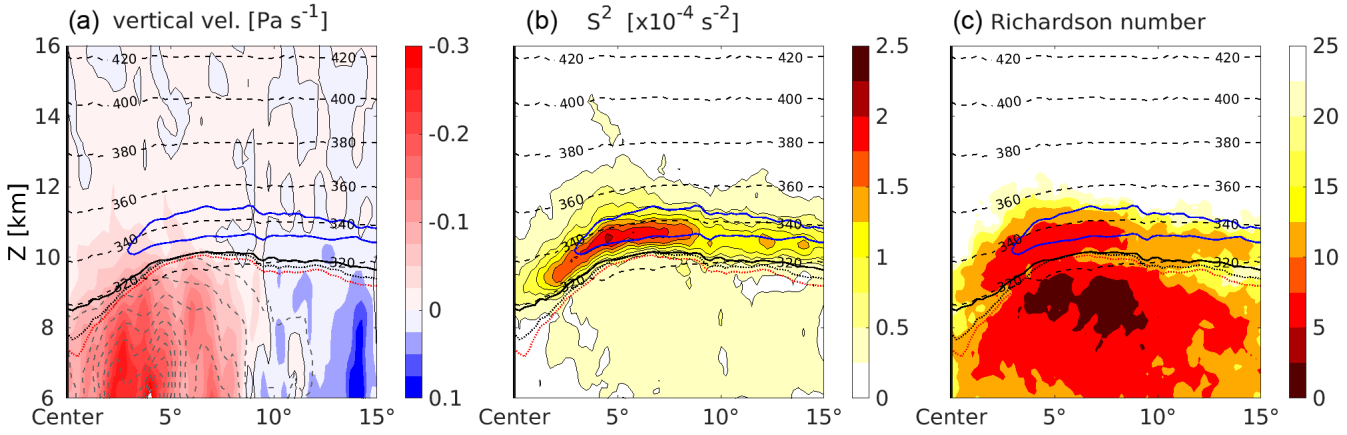

Figure 10. Vertical tropopause-based averaged cross-section as in ~~Figure 8~~Fig. 9, but only north of the cyclone centre. Left panel: filled contours show mean vertical velocity, solid thin black line the $\omega = 0$ Pa s^{-1} isoline. Grey dashed lines are isolines of the cloud ice water content, steps as in Fig. 9. Middle panel: filled contour and solid black contour lines show squared vertical shear of horizontal wind S^2. Right panel: modified Richardson number mean Ri, with an inverted color scale (red represents low values) to highlight the tendency toward turbulent motion. ~~Grey~~Blue solid bold line in all three panels shows the $N^2_{mean} = 6 \times 10^{-4}$ s^{-2} isoline, dashed black lines the isentropes.

develop in stably stratified flow with $Ri < Ri_c$. We calculate the modified Richardson number mean as described in Birner et al. (2002) who take the natural logarithm of the individual Richardson numbers before computing an average to reduce the variability range: $Ri' = \mathrm{sign}(N^2)\ln(|N^2|/S^2+1)$. The mean Richardson number is then calculated as $Ri = \exp(\overline{Ri'})-1$. The result is depicted in Fig. 10 and shows two regions of minimum mean Richardson numbers. The lowest values of Ri are evident in the upper troposphere in the upper regions of the ascending air masses which is a result of a very weak stratification combined with a moderately strong vertical wind shear due to a local maximum of the meridional wind component at tropopause height at about 7.5° N (not shown). A second region of minimum mean Richardson numbers is located right above the tropopause near the cyclone centre, and extends into the regions of maximum static stability. In this region the vertical wind shear S^2 is the dominating factor that works towards dynamic instability. This agrees well with one result from Birner et al. (2002) who saw a similar partly vertical overlap of a maximum in vertical wind shear and the TIL in radiosonde profiles. Grise et al. (2010) furthermore stated a fundamental link between the zonal-mean static stability and the zonal-mean zonal wind based on the thermal wind relation, highlighting a dependency between the meridional gradient of the static stability and the curvature of the vertical shear of the horizontal wind.

We furthermore tested different methods of calculating an average Richardson number to check the robustness of our result. Calculating the unmodified Richardson numbers for each individual cyclone and averaging afterwards produces a very fragmented mean field, but it still exhibits a region with local minima of the order of 10^1 inside the region of the TIL. Calculating the mean Richardson number from the averaged potential temperature and wind field yields a result more comparable to the modified Richardson mean, but with overall larger values for Ri, stronger separated minima, and sharper gradients of

Ri. Birner et al. (2002) observed a distinct discrepancy in the vertical shear of the horizontal wind S^2 above the tropopause between the radiosonde data and ECMWF reanalysis data. This shows that the vertical wind gradients in the UTLS are not well resolved and significantly underestimated by the reanalysis data, a tendency which might still be the case in the analysis data. The fact that we see a strong maximum in S^2 above the tropopause in NWP data, while Birner et al. (2002) saw none in the mean profiles from reanalysis data, can be explained by 1.) the finer vertical and horizontal resolution in the operational IFS model, and 2.) the fact that we present a composite of a specific synoptic situation which may result in a similar structure of the individual vertical profiles. ~~Richardson numbers of the order of 5-10 still represent a stable flow, but we want to stress that these are mean values from 76 cyclones, and based on vertical gradients of N^2 and S^2 derived from a vertical grid spacing of about $\Delta z \approx 300$ m.~~The lowermost stratosphere north of the cyclone centre exhibits Richardson numbers of $Ri = 5 - 10$ which are still well above the critical value of $Ri_c = 0.25$ for turbulent flow. These Richardson numbers however present an average of a highly non-linear measure over 76 cyclones. For individual cyclones Richardson numbers often exhibit much lower values in this region, eventually below the critical value Ri_c and thus are indicative for dynamic instability. Also we would like to remind the reader that these quantities are derived from model data with a vertical grid spacing of about $\Delta z \approx 300$ m. The two features of interest (N^2_{max} and S^2_{max}) typically exhibit a vertical extent of 1-3 km, therefore the model output profiles of N^2 and S^2 in the lowermost stratosphere can be expected to be a to a certain degree smoothed representation of the real atmosphere. A possible misrepresentation of the ratio between the two gradient-based measures N^2 and S^2 opens the possibility for an even larger range of Richardson numbers in the real flow. ~~Therefore~~In conclusion, there is the possibility that turbulence is present even in regions of enhanced static stability in the lower stratosphere which might affect cross tropopause transport in these regions.

~~Figure 12 provides a strong indication that a co-location between the regions of enhanced static stability above the tropopause and the maximum in vertical shear of the horizontal wind exists. Figure 12a shows the quasi-horizontal composite of the maximum in wind shear within 3 km above the tropopause for the subset of strong cyclones ($p_{msl,\,min} \leq 990$ hPa). It reveals together with Fig. 7 that there is a co-location between the regions of maximum squared wind shear S^2_{max} above the tropopause and the regions of maximum enhancement in static stability N^2_{max} in the lower stratosphere. Figure 12 furthermore shows how both features are also vertically constrained north of the cyclone centre, resulting in the vertical overlap of the wind shear region and the TIL (see also Fig. 9 and Fig. 10b).~~ Figure 11 further illustrates the connection between the regions of enhanced static stability and the vertical shear of the horizontal wind in the vicinity of cyclones. It shows the composite derived from the quasi-horizontal fields of maximum wind shear S^2_{max} found within 3 km above the tropopause in the 76 strong cyclones. The region of largest mean wind shear matches with the region of maximum enhanced static stability (see Fig. 7b), with maximum values north and northeast of the cyclone centre within the wrapped-up ridge. The southern regions exhibit weaker mean wind shear, and the minimum values of S^2_{max} are located around the cyclone centre.

Figure 12 shows tropopause based averaged vertical cross-sections that cover the distance from the cyclone centre to the spherical cap radius of 15° and are oriented in different cardinal directions as indicated in Fig 11. These plots complement Fig. 10b and Fig. 11 and further confirm a co-location as well as a co-occurence of the regions of maximum wind shear S^2_{max} and the regions of maximum enhanced static stability N^2_{max}. They furthermore illustrate the validity and representativity of the

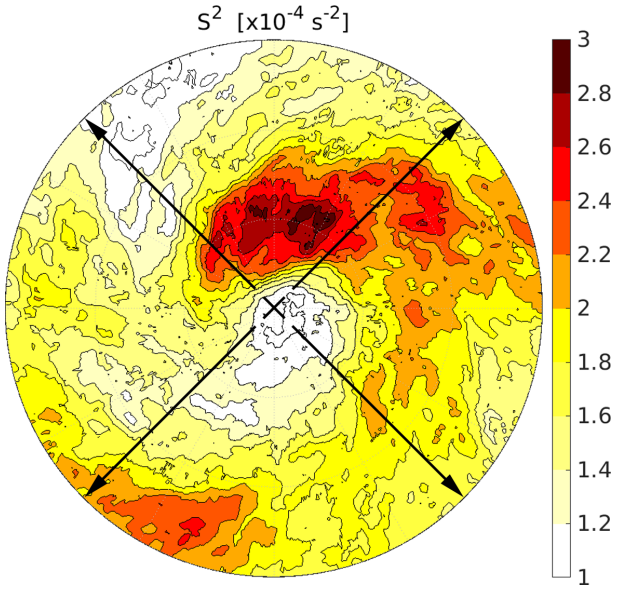

Figure 11. ~~Composite of flow features for the 76 strong cyclones with $p_{msl,\,min} \leq 990$ hPa at the point in time of maximum intensity. Left panel: composite of the maximum in vertical wind shear S^2_{max} found within 3 km above the lapse rate tropopause for each cyclone. The black arrow indicates the position of the vertical cross-sections in Fig. 9. Right panel: composite of the absolute height difference between the maximum in static stability N^2_{max} and the maximum in vertical wind shear S^2_{max}, both within 3 km above the lapse rate tropopause.~~ Composite of the vertical wind shear for the 76 strong cyclones with $p_{msl,\,min} \leq 990$ hPa at the point in time of maximum intensity, averaged over the individual quasi-horizontal fields of maximum vertical wind shear S^2_{max} found within 3 km above the lapse rate tropopause for each cyclone. The black arrows indicate the orientation of the vertical cross-sections in Fig. 12.

composites derived from the individual quasi-horizontal fields. The quasi-horizontal composite in Fig. 7b strongly depends on the definition of the TIL-strength (in this case the maximum value of N^2 within 3 km above the tropopause), while the vertical cross-section composites in the top row of Fig. 12 solely depend on the tropopause definition (equivalently Fig. 11 and Fig. 12 bottom row for the vertical wind shear). However, both methods show a good agreement, aside from an overall shift of the absolute values as expected and described in Sect. 2.2.1. Overall the composites give a comprehensive overview over the mean evolution of the TIL above surface cyclones and its relation with other flow features like tropospheric moist diabatic active regions or wind shear in the lower stratosphere.

5 Discussion and conclusions

The goal of this study was to analyse the development of the TIL during the evolution of baroclinic life cycles in operational ECMWF IFS analysis data. For this we tracked a total sum of 130 surface cyclones in the MSL pressure field over the North Atlantic from August to October during a five year period from 2010 to 2014. We presented an analysis of two consecutive

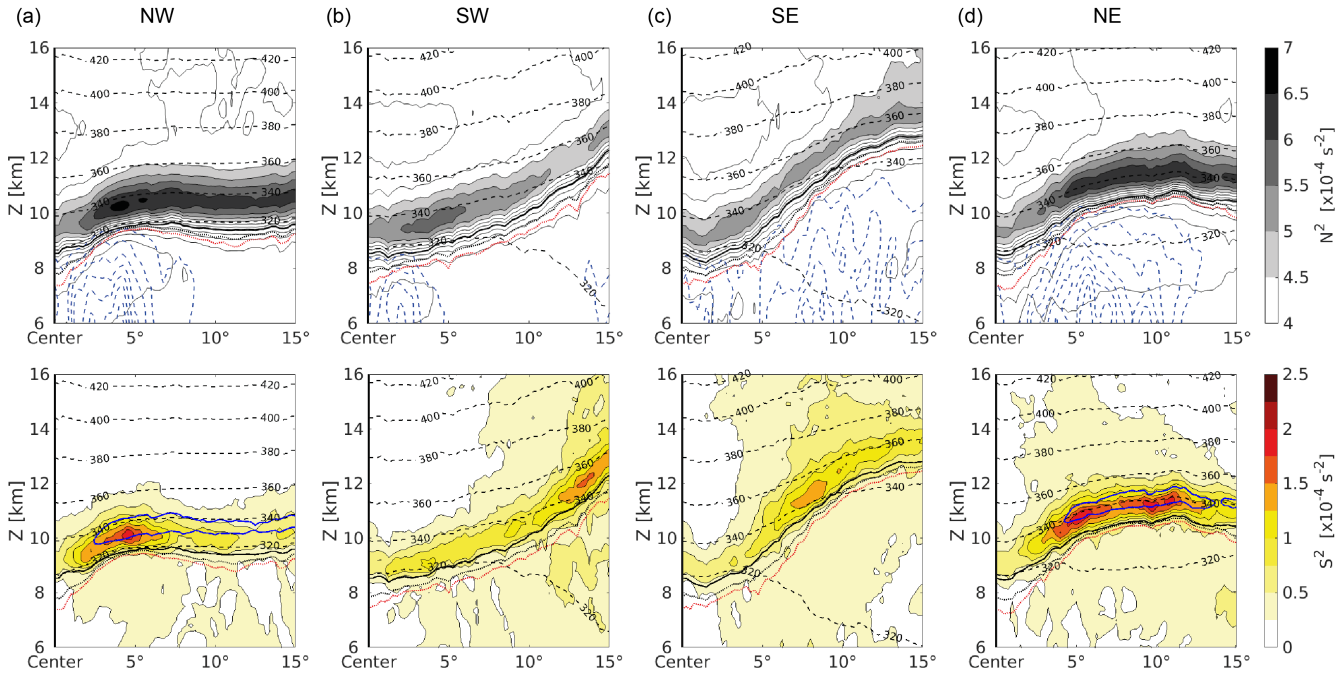

Figure 12. Composites of flow features for the 76 strong cyclones with $p_{msl,\,min} \leq 990$ hPa at the point in time of maximum intensity. Vertical tropopause-based averaged cross-section composites, reaching from the cyclone centre (a) northwestward, (b) southwestward, (c) southeastward and (e) northeastward. Top row shows static stability N^2 and cloud ice water content as in Fig. 9, bottom row shows wind shear S^2 as in Fig. 10b. The orientation of the vertical cross-sections is indicated by the black arrows in Fig. 11.

individual cyclones associated with two upper tropospheric baroclinic wave breaking events, one resembling an LC1 and the other one an LC2 event. We furthermore derived composites of the atmospheric state from different subsets of the 130 cyclones using the intensity of the surface cyclone as a selection criterion.

Based on the analysis of the two individual baroclinic life cycles (Sect. 3) in comparison with idealised baroclinic life cycle simulations from previous works (Wirth and Szabo, 2007; Erler and Wirth, 2011; Kunkel et al., 2014, 2016), we identified the regions of cyclonic wrap-up around the cyclone centre as the regions exhibiting the strongest signal in static stability above the lapse rate tropopause. The flow in the UTLS with relatively large values of isentropic potential vorticity and positive relative vorticity coming from northwest and wrapping up around the cyclone centre exhibits low values of static stability, while the counterpart of anticyclonic low-IPV air originating from lower latitudes shows a distinct enhancement in static stability and represents the region with a well developed TIL. The largest values of static stability above the tropopause are located north and northeast of the cyclone centre at about the time of maximum surface cyclone intensity. The synoptic scale TIL evolution in both the LC1 and LC2 baroclinic waves is similar, with differences in the strength and the shape of the region of the wrap-up. The relatively weak secondary cyclone associated with the cut-off which resulted from the LC1 wave breaking event shows a

similar evolution on a smaller horizontal scale. The TIL above the individual cyclones exhibits a large temporal, horizontal, and vertical variability on different scales associated to the variety of known forcing mechanisms being resolved in the high resolution NWP data.

Furthermore, we presented composites of the atmospheric state in the vicinity of different subsets of tracked cyclone centres at the point in time of maximum cyclone intensity. We find that stronger surface cyclones are associated with a sharper and more pronounced wrap-up in the UTLS flow. The composites furthermore resemble to a large degree the key features of the TIL evolution and the mean flow as identified from the case studies. The regions of largest TIL enhancement are located north and northeast of the cyclone centre ~~above the occlusion and~~ above regions influenced by strong tropospheric updrafts and clouds reaching up to the tropopause, where in this central stage of the baroclinic life cycle typically the warm conveyor belt outflow occurs (e.g., Madonna et al., 2014; Kunkel et al., 2016). The high reaching clouds ~~This~~ indicate~~s~~ the importance of moist dynamical and radiative processes during the formation of the TIL (e.g., Randel et al., 2007; Kunkel et al., 2016). The composites further reveal a maximum in vertical shear of the horizontal wind S^2 within the region of strongest enhancement of static stability above the tropopause. The regions of maximum static stability and those of maximum wind shear show a remarkable overlap, horizontally as well as vertically, which is in agreement with previous studies (Birner et al., 2002; Grise et al., 2010). Mean Richardson numbers calculated for these flow conditions ~~favourable for turbulence~~ reveal a region of local minima in Ri right above the tropopause at around 5° north from the cyclone centre in the composite. ~~This result points toward a co-location between an enhancement in static stability above the tropopause and potential turbulent mixing of tropospheric and stratospheric air masses (Kunkel et al., 2016).~~ Taking into account the variability of N^2 and S^2 for individual cyclones, this result points toward the possibility of a co-location between enhanced static stability above the tropopause and localised regions of turbulent mixing of tropospheric and stratospheric air masses (Kunkel et al., 2016).

We want to note that baroclinic life cycles vary in their appearance from case to case and thus the TIL evolution in individual cyclones can differ from the one described by the composite analysis. The analysis of baroclinic life cycles in other regions and seasons would of course be desirable, but is left open at this stage for later studies. The approach used in this study is now applicable to a large data set, e.g. using the new ERA-5 reanalysis which has the same vertical resolution in the UTLS as the analysis data in this study.

Overall this study confirms the importance of baroclinic waves and their embedded cyclones to explain the meso-scale variability of enhanced static stability above the lapse rate tropopause in the extratropics. The high spatial and temporal resolution of the analysis data gives a better understanding on where and when static stability increases during baroclinic life cycles. The composites of baroclinic life cycles show a large agreement of TIL evolution with the individual life cycles in the analysis data as well as with the individual life cycles from earlier idealised studies (Erler and Wirth, 2011; Kunkel et al., 2016). They furthermore indicate that turbulent mixing might occur in regions of enhanced static stability right above the tropopause.

Author contributions. DK, PH and TK designed the research project. TK developed the model code and performed the calculations, and analysed the data with the help of DK and PH. TK prepared the manuscript with contributions from all authors.

Competing interests. The authors declare that they have no conflict of interest.

Acknowledgements. The Authors acknowledge funding from the German Science Foundation, as this study was carried out as part of the preparation phase for the WISE campaign under funding from the HALO SPP 1294 (DFG grant no. KU 3524/1-1, HO 4225/7-1 as well as HO 4225/8-1). We are furthermore grateful to the ECMWF for providing the IFS analysis data which has been downloaded from the ECMWF MARS system.

References

Bengtsson, L., Hodges, K. I., Esch, M., Keenlyside, N., Kornblueh, L., Luo, J. J., and Yamagata, T.: How may tropical cyclones change in a warmer climate?, Tellus, Series A: Dynamic Meteorology and Oceanography, 59 A, 539–561, https://doi.org/10.1111/j.1600-0870.2007.00251.x, 2007.

Birner, T.: Fine-scale structure of the extratropical tropopause region, Journal of Geophysical Research Atmospheres, 111, 1–14, https://doi.org/10.1029/2005JD006301, 2006.

Birner, T.: Residual Circulation and Tropopause Structure, Journal of the Atmospheric Sciences, pp. 2582–2600, https://doi.org/10.1175/2010JAS3287.1, 2010.

Birner, T., Dörnbrack, A., and Schumann, U.: How sharp is the tropopause at midlatitudes?, Geophysical Research Letters, 29, 45–1–45–4, https://doi.org/10.1029/2002GL015142, 2002.

Catto, J. L., Shaffrey, L. C., and Hodges, K. I.: Can climate models capture the structure of extratropical cyclones?, Journal of Climate, 23, 1621–1635, https://doi.org/10.1175/2009JCLI3318.1, 2010.

Cressman, G. P.: an Operational Objective Analysis System, Monthly Weather Review, 87, 367–374, https://doi.org/10.1175/1520-0493(1959)087<0367:AOOAS>2.0.CO;2, 1959.

Erler, A. R. and Wirth, V.: The Static Stability of the Tropopause Region in Adiabatic Baroclinic Life Cycle Experiments, Journal of the Atmospheric Sciences, 68, 1178–1193, https://doi.org/10.1175/2010JAS3694.1, 2011.

Flaounas, E., Raveh-Rubin, S., Wernli, H., Drobinski, P., and Bastin, S.: The dynamical structure of intense Mediterranean cyclones, Climate Dynamics, 44, 2411–2427, https://doi.org/10.1007/s00382-014-2330-2, 2015.

Gettelman, A. and Wang, T.: Structural diagnostics of the tropopause inversion layer and its evolution, Journal of Geophysical Research Atmospheres, 120, 46–62, https://doi.org/10.1002/2014JD021846, 2015.

Gisinger, S., Dörnbrack, A., Matthias, V., Doyle, J. D., Eckermann, S. D., Ehard, B., Hoffmann, L., Kaifler, B., Kruse, C. G., Rapp, M., Gisinger, S., Dörnbrack, A., Matthias, V., Doyle, J. D., Eckermann, S. D., Ehard, B., Hoffmann, L., Kaifler, B., Kruse, C. G., and Rapp, M.: Atmospheric Conditions during the Deep Propagating Gravity Wave Experiment (DEEPWAVE), Monthly Weather Review, 145, 4249–4275, https://doi.org/10.1175/MWR-D-16-0435.1, 2017.

Grise, K. M., Thompson, D. W., and Birner, T.: A global survey of static stability in the stratosphere and upper troposphere, Journal of Climate, 23, 2275–2292, https://doi.org/10.1175/2009JCLI3369.1, 2010.

Hanley, J. and Caballero, R.: Objective identification and tracking of multicentre cyclones in the ERA-Interim reanalysis dataset, Quarterly Journal of the Royal Meteorological Society, 138, 612–625, https://doi.org/10.1002/qj.948, 2012.

Hegglin, M. I., Boone, C. D., Manney, G. L., and Walker, K. A.: A global view of the extratropical tropopause transition layer from Atmospheric Chemistry Experiment Fourier Transform Spectrometer O3, H2O, and CO, Journal of Geophysical Research Atmospheres, 114, 1–18, https://doi.org/10.1029/2008JD009984, 2009.

Hoor, P., Fischer, H., Lange, L., Lelieveld, J., and Brunner, D.: Seasonal variations of a mixing layer in the lowermost stratosphere as identified by the CO-O ₃ correlation from in situ measurements, Journal of Geophysical Research: Atmospheres, 107, ACL 1–1–ACL 1–11, https://doi.org/10.1029/2000JD000289, 2002.

Hoor, P., Gurk, C., Brunner, D., Hegglin, M. I., Wernli, H., and Fischer, H.: Seasonality and extent of extratropical TST derived from in-situ CO measurements during SPURT, Atmospheric Chemistry and Physics Discussions, 4, 1691–1726, https://doi.org/10.5194/acpd-4-1691-2004, 2004.

Kunkel, D., Hoor, P., and Wirth, V.: Can inertia-gravity waves persistently alter the tropopause inversion layer?, Geophysical Research Letters, 41, 7822–7829, https://doi.org/10.1002/2014GL061970, 2014.

Kunkel, D., Hoor, P., and Wirth, V.: The tropopause inversion layer in baroclinic life-cycle experiments: The role of diabatic processes, Atmospheric Chemistry and Physics, 16, 541–560, https://doi.org/10.5194/acp-16-541-2016, 2016.

Kunz, A., Konopka, P., Müller, R., Pan, L. L., Schiller, C., and Rohrer, F.: High static stability in the mixing layer above the extratropical tropopause, Journal of Geophysical Research Atmospheres, 114, 1–9, https://doi.org/10.1029/2009JD011840, 2009.

Madonna, E., Wernli, H., Joos, H., and Martius, O.: Warm conveyor belts in the ERA-Interim Dataset (1979-2010). Part I: Climatology and potential vorticity evolution, Journal of Climate, 27, 3–26, https://doi.org/10.1175/JCLI-D-12-00720.1, 2014.

Neu, U., Akperov, M. G., Bellenbaum, N., Benestad, R., Blender, R., Caballero, R., Cocozza, A., Dacre, H. F., Feng, Y., Fraedrich, K., Grieger, J., Gulev, S., Hanley, J., Hewson, T., Inatsu, M., Keay, K., Kew, S. F., Kindem, I., Leckebusch, G. C., Liberato, M. L. R., Lionello, P., Mokhov, I. I., Pinto, J. G., Raible, C. C., Reale, M., Rudeva, I., Schuster, M., Simmonds, I., Sinclair, M., Sprenger, M., Tilinina, N. D., Trigo, I. F., Ulbrich, S., Ulbrich, U., Wang, X. L., and Wernli, H.: Imilast: A community effort to intercompare extratropical cyclone detection and tracking algorithms, Bulletin of the American Meteorological Society, 94, 529–547, https://doi.org/10.1175/BAMS-D-11-00154.1, 2013.

Pan, L. L., Randel, W. J., Gary, B. L., Mahoney, M. J., and Hintsa, E. J.: Definitions and sharpness of the extratropical tropopause: A trace gas perspective, Journal of Geophysical Research D: Atmospheres, 109, 1–11, https://doi.org/10.1029/2004JD004982, 2004.

Pilch Kedzierski, R., Matthes, K., and Bumke, K.: Synoptic-scale behavior of the extratropical tropopause inversion layer, Geophysical Research Letters, 42, 10 018–10 026, https://doi.org/10.1002/2015GL066409, 2015.

Pilch Kedzierski, R., Matthes, K., and Bumke, K.: Wave modulation of the extratropical tropopause inversion layer, Atmospheric Chemistry and Physics, 17, 4093–4114, https://doi.org/10.5194/acp-17-4093-2017, 2017.

Randel, W. J., Wu, F., and Forster, P.: The Extratropical Tropopause Inversion Layer: Global Observations with GPS Data, and a Radiative Forcing Mechanism, Journal of the Atmospheric Sciences, 64, 4489–4496, https://doi.org/10.1175/2007JAS2412.1, 2007.

Schmidt, T., Cammas, J. P., Smit, H. G., Heise, S., Wickert, J., and Haser, A.: Observational characteristics of the tropopause inversion layer derived from CHAMP/GRACE radio occultations and MOZAIC aircraft data, Journal of Geophysical Research Atmospheres, 115, 1–16, https://doi.org/10.1029/2010JD014284, 2010.

Sjoberg, J. P. and Birner, T.: Stratospheric Wave–Mean Flow Feedbacks and Sudden Stratospheric Warmings in a Simple Model Forced by Upward Wave Activity Flux, Journal of the Atmospheric Sciences, 71, 4055–4071, https://doi.org/10.1175/JAS-D-14-0113.1, 2014.

Son, S. W. and Polvani, L. M.: Dynamical formation of an extra-tropical tropopause inversion layer in a relatively simple general circulation model, Geophysical Research Letters, 34, 1–5, https://doi.org/10.1029/2007GL030564, 2007.

Thorncroft, C. D., Hoskins, B. J., and McIntyre, M. E.: Two paradigms of baroclinic-wave life-cycle behaviour, Quarterly Journal of the Royal Meteorological Society, 119, 17–55, https://doi.org/10.1002/qj.49711950903, 1993.

Wang, C.-C. and Rogers, J. C.: A Composite Study of Explosive Cyclogenesis in Different Sectors of the North Atlantic. Part I: Cyclone Structure and Evolution, Monthly Weather Review, 129, 1481–1499, https://doi.org/10.1175/1520-0493(2001)129<1481:ACSOEC>2.0.CO;2, 2001.

Wernli, H. and Schwierz, C.: Surface Cyclones in the ERA-40 Dataset (1958–2001). Part I: Novel Identification Method and Global Climatology, Journal of the Atmospheric Sciences, 63, 2486–2507, https://doi.org/10.1175/JAS3766.1, 2006.

Wirth, V.: Static Stability in the Extratropical Tropopause Region, Journal of the Atmospheric Sciences, 60, 1395–1409, https://doi.org/10.1175/1520-0469(2003)060<1395:SSITET>2.0.CO;2, 2003.

Wirth, V.: A dynamical mechanism for tropopause sharpening, Meteorologische Zeitschrift, 13, 477–484, https://doi.org/10.1127/0941-2948/2004/0013-0477, 2004.

Wirth, V. and Szabo, T.: Sharpness of the extratropical tropopause in baroclinic life cycle experiments, Geophysical Research Letters, 34, 10–13, https://doi.org/10.1029/2006GL028369, 2007.

WMO: Meteorology - A three dimensional science, WMO Bulletin, pp. 134–138, 1957.